June 2026

NEW MEXICO STATEWIDE DROUGHT VULNERABILITY ANALYSIS UNDER FUTURE CLIMATE CHANGE SCENARIOS USING A PHYSICALLY BASED COUPLED MODEL

NM WRRI Technical Completion Report No. 413

Huidae Cho
Abdullah Azzam

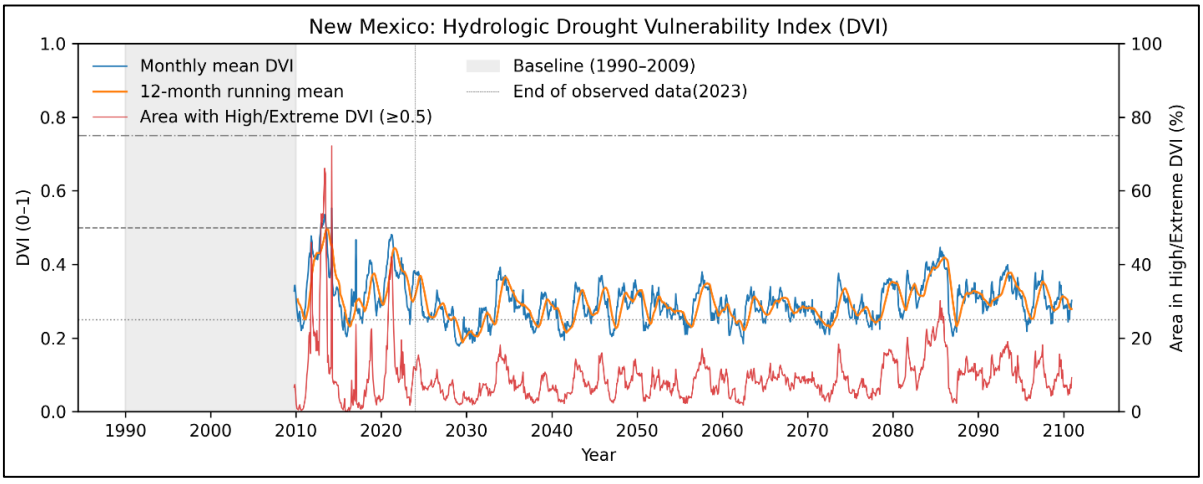

Statewide Monthly Mean DVI (blue), 12-Month Running Mean (orange), and Statewide Area in High/Extreme DVI (≥ 0.5, red). The shaded region marks the training baseline (1990–2009). Horizontal dashed lines indicate DVI thresholds of 0.25, 0.50, and 0.75, corresponding to increasing levels of drought vulnerability.

New Mexico Water Resources Research Institute
New Mexico State University
MSC 3167, P.O. Box 30001
Las Cruces, New Mexico 88003-0001
(575) 646-4337 email: nmwrri@nmsu.edu

NEW MEXICO STATEWIDE DROUGHT VULNERABILITY ANALYSIS UNDER FUTURE CLIMATE CHANGE SCENARIOS USING A PHYSICALLY BASED COUPLED MODEL

By

Huidae Cho, Associate Professor
Abdullah Azzam, Graduate Student

Department of Civil and Environmental Engineering
New Mexico State University

TECHNICAL COMPLETION REPORT
Account Number GR0007017
Technical Completion Report #413

June 2026

New Mexico Water Resources Research Institute
in cooperation with the
Department of Civil and Environmental Engineering
New Mexico State University

The research on which this report is based was supported by the U.S. Department of the Interior, Geological Survey through the New Mexico Water Resources Research Institute under Grant/Cooperative Agreement No. G21AP10635.

Page Intentionally Left Blank

DISCLAIMER

The purpose of the NM Water Resources Research Institute (NM WRRI) technical reports is to provide a timely outlet for research results obtained on projects supported in whole or in part by the institute. Through these reports the NM WRRI promotes the free exchange of information and ideas and hopes to stimulate thoughtful discussions and actions that may lead to resolution of water problems. The NM WRRI, through peer review of draft reports, attempts to substantiate the accuracy of information contained within its reports, but the views and conclusions contained in this document are those of the authors and should not be interpreted as representing the opinions or policies of the U.S. Geological Survey. Mention of trade name or commercial products does not constitute their endorsement by the U.S. Geological Survey. This manuscript is submitted for publication with the understanding that the United States Government is authorized to reproduce and distribute reprints for Governmental purposes.

ABSTRACT

New Mexico, one of the fastest-warming states in the United States, faces increasing challenges in managing water resources because of declining snowpack and intensified groundwater extraction. The goal of this project was to assess drought vulnerability for the entire state using historical and forecasted climate data from 1940 to 2100. Specifically, the objectives were to: (1) determine an appropriate spatial resolution for statewide hydrologic modeling, (2) develop a computationally feasible coupled surface–subsurface hydrologic model, (3) implement distributed computing techniques for large-scale optimization, (4) forecast drought conditions to 2100 with associated uncertainty using CMIP6 climate projections, and (5) calculate a statewide Drought Vulnerability Index (DVI) to inform water resources management.

To achieve these objectives, we developed a high-resolution, fully automated hydrologic modeling framework VIC-MF6 that couples the Variable Infiltration Capacity (VIC) surface water model with the MODFLOW 6 (MF6) groundwater model. The VIC-MF6 framework operates at a spatial resolution of 1/32° (~3 km) and integrates observed and projected climate data from 1940 to 2100. Automated modules handle parameter downscaling, data conversion, and model synchronization via the MF6 Application Programming Interface (API) based on the eXtended Model Interface (XMI), allowing monthly exchange of baseflow and groundwater discharge. The framework was applied over the domain of the Rio Grande Transboundary Integrated Hydrologic Model (RGTIHM) and demonstrated scalability, computational efficiency, and physical consistency.

The statewide DVI reproduces observed drought episodes from 2010–2023, including 2011–2013, 2018, and 2020–2021, with strong agreement with U.S. Drought Monitor data. Historical statewide monthly mean DVI shows high interannual variability, with 12-month running means peaking around 2011–2013, when areas in high/extreme DVI (≥ 0.5) briefly exceeded 50%, and 2020–2021. After 2024, the smoothed DVI remains lower and more stable, with typical peaks below ~0.4 and high/extreme coverage under 20%. Spatially, historical mean DVI (1991–2024) is low to moderate and relatively homogeneous, while future mean DVI (2025–2100) increases in northern and west-central mountains (up to +0.3) and decreases in central and eastern plains (down to −0.3), indicating a redistribution of vulnerability rather than a uniform increase. The frequency of high-vulnerability months mirrors this pattern, increasing in headwater regions

while remaining low elsewhere. Month-to-month DVI class transition probabilities show strong persistence (91.5% low, 90.7% moderate, 87.0% high, 72.6% extreme), supporting the use of backward windows and demonstrating gradual relaxation of extreme events. Distribution analysis reveals a lower future median DVI (~0.26 vs. ~0.32 historically) with increased spatial spread, reinforcing greater heterogeneity across grid cells.

These results indicate that, although the statewide average drought vulnerability may decline under projected climate conditions, high-elevation basins face increasing and more persistent risk. The findings provide quantitative, spatially explicit insight into New Mexico's drought vulnerability and offers a robust foundation for region-specific water resources management strategies and long-term planning.

Keywords

New Mexico, drought vulnerability, surface–subsurface hydrologic coupling, VIC, MODFLOW 6, hydrologic modeling framework, parallel computing.

TABLE OF CONTENTS

LIST OF FIGURES

LIST OF TABLES

1. INTRODUCTION

1.1. Background and Motivation

New Mexico, identified as the sixth fastest-warming state in the United States, faces significant challenges in managing water resources under amplified hydroclimatic variability, particularly with increasing drought frequency and severity (Union of Concerned Scientists, 2016). Snowmelt-derived surface flows and groundwater withdrawals constitute the primary water sources for municipal and agricultural demands, particularly in the Rio Grande Basin. These hydrologic systems are intricately linked through complex surface–subsurface interactions that vary across spatial and temporal scales. Without integrated, predictive modeling tools, water resources managers and planners can face difficulties in quantifying the long-term impacts of warming trends, reduced snowpack, and intensified groundwater extraction on water availability.

Previous studies have addressed components of New Mexico's hydrology using standalone or loosely coupled models. Ketchum (2016) estimated groundwater recharge across the state from 2000 to 2013 using a daily soil-water balance model informed by remote sensing datasets. Xu (2018) refined this approach by improving the estimation of focused recharge. However, these studies emphasized historical simulations and did not provide forward-looking projections, which are critical for long-term planning. Moreover, integrating surface and subsurface hydrology at a statewide scale remains challenging because of the complexity of coupling processes, heterogeneity in data formats, and substantial computational requirements.

Recent advancements in coupled hydrologic modeling have demonstrated the potential for integrated approaches. Jafari et al. (2021) coupled the Soil and Water Assessment Tool (SWAT) (Arnold et al., 1998) with MODFLOW (Langevin et al., 2017), a groundwater model developed by USGS, to simulate surface–subsurface hydrologic interactions in a 1,452 km^2 watershed, identifying curve number and hydraulic conductivity as key parameters. Similarly, Sridhar et al. (2018) integrated the Variable Infiltration Capacity (VIC) model (Hamman et al., 2018), a macroscale land surface model, with MODFLOW to improve streamflow predictions in a 186,479 km^2 watershed in Idaho. Their results underscored the value of coupled modeling frameworks for capturing complex hydrologic dynamics and informing sustainable watershed management practices.

Despite these successes, prior studies have been limited in spatial and temporal scope mainly because of computational constraints. For instance, Sridhar et al. (2018) focused on a 27,972 km^2 aquifer region and a 5-year calibration period, which restricts the applicability of their framework for larger-scale, long-term hydrologic assessment. Given that New Mexico encompasses approximately 314,000 km^2 with diverse topography and hydrologic regimes, there is a critical need for a scalable, automated, and computationally efficient hydrologic modeling framework capable of simulating statewide surface–subsurface interactions over multi-decadal periods. In response, this study focused on developing a high-resolution, fully automated software framework that couples the VIC surface model with MODFLOW 6 (MF6) (Langevin et al., 2017), integrating observed and projected climate data, parameter downscaling, data conversion, and model synchronization. The resulting framework offers the computational efficiency and scalability required to support large-scale drought vulnerability assessments and water resources planning, while providing a foundation for future expansion of coupled surface–subsurface modeling across the entire state.

1.2. Goals, Objectives, and Contributions

The overarching goal of this study was to evaluate statewide drought vulnerability in New Mexico under historical and projected climate conditions from 1940 to 2100, using physically based hydrologic modeling. This assessment aimed to provide spatially and temporally explicit information to support long-term water resources planning and sustainable management in the rapidly warming and water-limited state. To achieve this goal, the primary objective was to develop a statewide high-resolution, fully automated software framework that couples the VIC land surface model with the MF6 groundwater model. This coupled VIC-MF6 framework enables simulation of both surface and subsurface water dynamics, their interactions, and responses to climatic variability, with statewide surface-water modeling and coupled surface–subsurface modeling currently implemented for the Lower Rio Grande Basin. By bridging high-resolution, physically based hydrologic modeling with practical, large-scale water resources management, this framework offers a scalable tool for understanding and mitigating drought vulnerability in New Mexico.

We achieved the project objectives by leveraging the capabilities of the coupled VIC-MF6 framework. The framework provides support for researchers and decision makers to:

1. Simulate historical and projected hydrologic conditions, including surface runoff, baseflow, and groundwater recharge and discharge,
2. Represent topographic heterogeneity across New Mexico and hydrogeologic heterogeneity within the modeled Lower Rio Grande Basin domain, including headwater regions, plains, and mountain basins,
3. Incorporate computational efficiency and automation through the MF6 Application Programming Interface (API) and eXtended Model Interface (XMI) to enable robust, reproducible, and scalable coupled simulations of statewide surface-water and Lower Rio Grande Basin groundwater systems,
4. Conduct multi-decadal drought vulnerability assessment using a Drought Vulnerability Index (DVI) standardized to a fixed historical baseline, and
5. Support decision-making and planning with temporally consistent, physically based assessments of drought risk under both historical variability and future climate projections.

These capabilities allowed the project to meet its proposed objectives:

1. Determine an appropriate spatial resolution for statewide hydrologic modeling,
2. Develop a computationally feasible coupled surface–subsurface hydrologic model,
3. Implement distributed computing techniques for large-scale optimization,
4. Forecast drought conditions to 2100 with associated uncertainty using Coupled Model Intercomparison Project Phase 6 (CMIP6) climate projections, and
5. Calculate a statewide DVI to inform water resources management and drought planning.

Key contributions through this research include:

1. A reproducible workflow that supports data preprocessing, model configuration, and execution, with support for scripting and version tracking,
2. A set of conversion tools to transition from legacy or incompatible formats (e.g., VIC Classic, MODFLOW One-Water Hydrologic Flow Model [MF-OWHM]) to scalable, NetCDF-based or parallelization-compatible formats required for surface–subsurface coupling (e.g., VIC Image, MF6),
3. A coupling controller VIC-MF6 that links surface and subsurface processes using the MF6 XMI, allowing exchange of hydrologic fluxes and states such as groundwater discharge and baseflow at each simulation stress period,

4. An application of the coupled VIC-MF6 framework, featuring statewide surface-water simulations and Lower Rio Grande Basin groundwater simulations over the historical period from 1940 to 2024 using observed meteorological data, and extended through 2100 using downscaled CMIP6 (Eyring et al., 2016) climate projections, with VIC simulations conducted at a spatial resolution of 1/32°, and
5. A statewide DVI to evaluate future drought vulnerability in the state to inform water resources decision makers.

1.3. Framework Architecture Overview

The full modeling framework developed in this study comprises four integrated software components:

1. VIC Input Generation Pipeline: A modular preprocessing system built using the Geographic Resources Analysis Support System (GRASS) (GRASS Development Team et al., 2025), involving shell scripts and custom C programs, that generates all VIC input layers (soil, vegetation, meteorology, Leaf Area Index [LAI]). This pipeline supports generalized applications to any domain given appropriate source datasets.
2. VIC Classic to VIC Image Converter: A dedicated C program that translates VIC Classic text-based input files into VIC Image NetCDF input files, enabling spatially parallel simulation and flux exchange. The tool automates input parsing, domain generation, and parameter transformation.
3. The Rio Grande Transboundary Integrated Hydrologic Model (RGTIHM) (Hanson et al., 2020) to MF6 Converter: A Python-based system built using FloPy (Bakker et al., 2016) that parses the original MF-OWHM (Hanson et al., 2014) implementation of the RGTIHM and generates a functionally equivalent MF6 model. The converter preserves all MF6-compatible inputs, including stress periods, wells, grid geometries, and boundary conditions, and produces spatial verification layers in the GeoPackage format.
4. VIC-MF6 Coupling Controller: A Python module that synchronizes VIC and MF6 model execution at each time step using the XMI. This component handles state management, water balance checking, and file Input/Output (I/O) between VIC's NetCDF outputs and MF6's recharge and baseflow fields.

1.4. Broader Impact and Use Case

To demonstrate its performance and applicability, the coupled framework was deployed for surface water across the entire state of New Mexico, with a groundwater focus on the Lower Rio Grande Basin as defined by the RGTIHM. Model simulations spanned the historical period from 1940 to 2024, with future scenario support available through climate-forcing extensions until 2100. To the best of our knowledge, this study presents the first successful integration of statewide surface-water modeling and Lower Rio Grande Basin groundwater modeling within a fully coupled, open-source, and scalable hydrologic simulation framework. We plan to extend the subsurface domain to include the Middle Rio Grande Basin as well.

Beyond hydrologic simulation, the framework supports statewide drought vulnerability analysis through the DVI. By combining VIC-derived fields such as precipitation, runoff, evapotranspiration, soil moisture, baseflow, and snowpack into a standardized index, the system provides a consistent and scalable way to track drought vulnerability over both historical and future periods. This integration allows statewide and basin-level assessments of drought exposure, persistence, and recovery, making the framework a versatile tool for climate adaptation research.

By integrating coupled hydrologic simulation with statewide drought vulnerability analysis, the framework advances both methodological innovation and practical decision support. It provides water managers and policymakers with a scalable tool to evaluate the combined impacts of groundwater stress and drought persistence across diverse hydroclimatic settings. As such, the system is well positioned to inform sustainable water resources planning, drought preparedness, and transboundary basin management in arid and semi-arid regions.

2. METHODS AND DATA

This section describes the methods and data used to develop the VIC-MF6 coupled hydrologic modeling framework for New Mexico. Figure 1 shows the flowchart for the overall methods that this project used for coupled hydrologic modeling and DVI computation. The project started with two existing calibrated models: (1) the Contiguous United States (CONUS) VIC surface water model by Yang et al. (2019) and (2) the RGTIHM groundwater model by Hanson et al. (2020). We coupled both calibrated models and used the results from the coupled simulation to calculate the DVI.

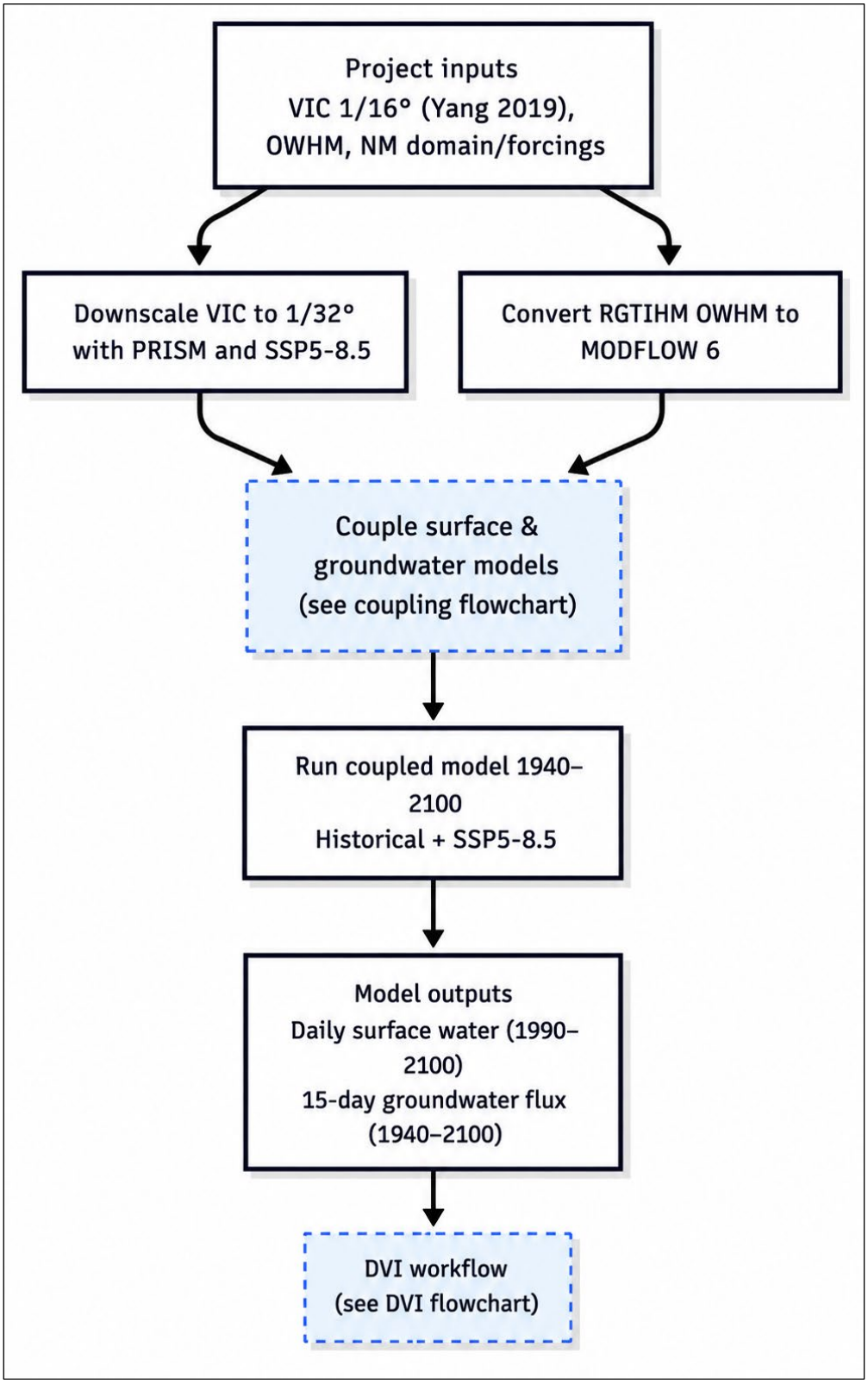

Figure 1. Flowchart for the Overall Methods of the Study.

Section 2.1 reviews foundational groundwater modeling studies, including the Lower Rio Grande (LRG) RGTIHM (Hanson et al., 2020) and the Middle Rio Grande (MRG) Basin MODFLOW model (McAda and Barroll, 2002). It describes the hydrogeologic structure, groundwater flow patterns, and key stresses such as pumping and recharge. The section also explains the conversion of the original RGTIHM from MF-OWHM to MF6 to support integration with parallelizable modeling workflows.

Section 2.2 describes the configuration of the surface water model using VIC. It outlines the spatial domain, model resolution, and parameter downscaling methods. The section also presents the preparation of meteorological forcing data consistent with the spatial and temporal requirements of the coupled framework. The methods described in this section were applied to determine an appropriate spatial resolution for statewide hydrologic modeling (Objective 1).

Section 2.3 presents the approach used for hydrologic forecasting under future climate conditions. It describes the use of downscaled CMIP6 projections to provide temperature, precipitation, and radiation inputs for the hydrological model and extrapolation of some inputs for the future. These data enable long-term simulations to evaluate the potential impacts of climate variability on regional hydrology. The methods and data in this section were used to forecast drought conditions through 2100 with associated uncertainty (Objective 4).

Section 2.4 details the architecture of the coupled modeling framework developed to automate and manage model workflows. It introduces the use of GRASS for spatial preprocessing, shell and Python scripts for automation, and C programs for raster data handling. The section also describes the implementation of the coupled VIC-MF6 simulation loop, designed to support high-resolution, long-term analysis across the study domain. This section contributes to the development of a computationally feasible coupled surface–subsurface hydrologic model (Objective 2) and supports the implementation of distributed computing techniques for large-scale optimization (Objective 3).

Section 2.5 explains the methods used to calculate the statewide DVI. It outlines the rationale underlying the drought vulnerability analysis approach and provides detailed procedures for DVI computation. This section provides the basis for calculating a statewide DVI to inform water resources management (Objective 5).

2.1. Groundwater Modeling

We adopted MF6 as the groundwater model for this study. MF6 is a modular, finite-difference groundwater flow model designed for flexible, large-scale hydrologic applications. Its object-oriented structure supports multiple groundwater flow models within a single simulation domain, enabling adaptive spatial resolution critical for New Mexico's heterogeneous aquifers. MF6's parallelization, implemented via the Message Passing Interface (MPI) (Forum, 1994), optimizes performance on High-Performance Computing (HPC) environments, making it suitable for large-scale statewide modeling. The model supports unstructured grids, enhancing computational efficiency and accuracy in representing complex hydrogeologic conditions, such as those in the Rio Grande Basin. Sections 2.1.1–2.1.7 summarize the methods and findings of Hanson et al. (2020) for Rio Grande transboundary hydrologic modeling. Section 2.1.8 discusses our efforts to convert the LRG (RGTIHM) model to MF6.

2.1.1. Rio Grande Transboundary Hydrology

The RGTIHM (Hanson et al., 2020) was designed to simulate the movement and use of groundwater in the Transboundary Rio Grande (TRG) region, which is considered the LRG region of the U.S. Developed using the MF-OWHM version 2, it integrates surface and groundwater systems to analyze water use, availability, and movement within the active model domain. The model provides a comprehensive tool for stakeholders to evaluate surface water operations and address water use issues in the region. Originally calibrated for the period 1940–2014, the RGTIHM requires periodic updates as hydrologic conditions evolve and new data become available. The development of the RGTIHM followed a three-phase approach:

1. Data collection and compilation,
2. Development of a hydrogeologic framework, and
3. Construction and calibration of the hydrologic model.

To refine the hydrologic representation, the model incorporates the Basin Characterization Model (BCM) to account for precipitation, recharge, and runoff during both dry and wet periods from 1940 to 2014. Key features of the RGTIHM include:

- Integration of surface water and groundwater interactions,
- Estimation of tributary boundary inflows from ephemeral streams,
- Simulation of supply-constrained and demand-driven water use, and
- Automated calibration using PEST software for model refinement.

2.1.2. Spatial and Temporal Configuration of the RGTIHM

The RGTIHM covers 1,760 mi^2 with a finite-difference grid consisting of 912 rows and 328 columns (299,136 cells) across nine geologic layers, totaling 816,886 active cells. A horizontal resolution of 10 ac per cell (201 m by 201 m) was selected to enhance accuracy in land use and water supply characterization. The grid is rotated 24° west of the north to align with regional geological features. The model layers correspond to five hydrogeologic units described by Sweetkind (2017) with the uppermost aquifer layer ranging from 50 ft to 110 ft thick and the deepest layer representing pre-Santa Fe Group rocks, varying between 500 ft and 607 ft in thickness. Temporally, the RGTIHM employs monthly stress periods and semi-monthly time steps, spanning 74.8 years from March 1940 to December 2014. Hanson et al. (2020) visualize the study area in great detail.

2.1.3. Groundwater Flow and Structural Influences

Groundwater flows from upland areas toward the Rio Grande through the Santa Fe Group of aquifers, primarily moving from northwest to the southeast. Structural features such as bedrock uplifts and faults influence flow patterns, creating distinct groundwater subregions. Historical data shows steep hydraulic gradients, with water moving from the Black Range and Caballo Mountains toward the Rincon Valley and Mesilla Basin.

2.1.4. Effects of Pumping and Recharge Sources

Since the 1950s, increasing agricultural and municipal groundwater withdrawals have altered groundwater-flow patterns in the Mesilla Basin, resulting in groundwater-level declines and the development of regional cones of depression in heavily pumped areas (Hanson et al., 2020). Seasonal declines in groundwater levels are linked to agricultural, municipal, and industrial withdrawals. Groundwater recharge sources include precipitation, streamflow, irrigation, and subsurface inflows, while outflows occur through pumping, evapotranspiration, and baseflow into streams. The El Paso Narrows act as a barrier, limiting groundwater movement from the Mesilla Basin into the Hueco Bolson. The main recharge source, apart from precipitation, is the surface water from the Rio Grande and its tributaries. This water resource is expressed as a surface water network in the SFR2 package in the MF-OWHM, which contains 566 segments, represented by 9,774 reaches, 61 diversions, 98 inflows, and 3 outflows.

2.1.5. Groundwater Use Trends

According to Hanson et al. (2020), groundwater irrigation in the TRG region expanded rapidly from the 1950s on because of drought, with the number of wells increasing from 11 in 1946 to over 1,000 by 1957. Currently, there are around 3,744 irrigation wells in New Mexico and 215 in Texas, though their operational status is uncertain. The RGTIHM includes a total of 14,698 wells, categorized into agriculture (509 single- and 3,450 multi-aquifer farm wells), municipal and industrial (1,874 wells), and domestic (8,865 wells). Agricultural groundwater withdrawals have fluctuated with climate conditions, peaking during droughts. In Doña Ana County, usage dropped from 73,000 ac-ft in 1975 to about 57,000–58,000 ac-ft in the wet 1980s but surged to 95,000 ac-ft in the early 2000s. Withdrawals in the LRG district doubled from 140,000 ac-ft in 2010 to 280,000 ac-ft in 2011, highlighting increasing reliance on groundwater.

2.1.6. Groundwater Pumping

Municipal and industrial groundwater pumping in the TRG region has increased since the 1940s, peaking in New Mexico at 64,000 ac-ft in 2009 because of population growth. In Texas, pumpage peaked at 28,000 ac-ft around 2000, while municipal pumping in Mexico began in 2010 and continues to rise. Major users include Las Cruces, El Paso, and the Camino Real Regional Utility Authority. Several smaller utilities also contribute, with 1,414 wells in New Mexico, 427 in Texas, and 33 in Chihuahua, Mexico. These trends can be observed in Hanson et al. (2020).

2.1.7. Domestic and Small-Scale Groundwater Use

Domestic well pumpage in Doña Ana County decreased from approximately 2,300 ac-ft in 1990 to 650 ac-ft in 2010, based on estimates compiled by the New Mexico Office of the State Engineer (NMOSE). The NMOSE reported 8,817 domestic wells in the New Mexico portion of the TRG region, but detailed information on active wells was scarce, making it difficult to determine the exact number of active wells. The Texas Water Development Board (TWDB) reported 60 domestic wells in the Texas part of the region. Similarly, the exact number of active wells was unclear. The RGTIHM plays a crucial role in advancing the understanding of groundwater dynamics in the Rio Grande Basin, facilitating better decision-making for water resources management in the transboundary region.

2.1.8. Conversion of the RGTIHM from the MF-OWHM to MF6

To leverage the RGTIHM's calibrated parameters, we converted its MF-OWHM implementation to MF6 for the 1940–2014 period. The conversion using the FloPy Python package (explained in Section 2.4) preserved the RGTIHM's grid geometry (201 m by 201 m), stress periods, well configurations, and boundary conditions, including recharge and flow barriers.

2.2. Surface Water Modeling

We used the VIC version 5 model to simulate surface water for this study. VIC is a grid-based, semi-distributed hydrologic model that is well-suited for large-scale, high-resolution surface water simulations. VIC provides physically based representations of key hydrologic processes, including evapotranspiration, soil moisture storage, baseflow generation, and snowpack dynamics, which is particularly critical for hydrologic modeling in New Mexico's mountainous regions. The model's ability to explicitly represent energy balance and snow accumulation/melt processes makes it ideal for snow-fed river systems in arid and semi-arid regions. VIC operates on a spatially distributed grid, allowing high-resolution simulations where each grid cell functions as an independent hydrologic unit while maintaining lateral water movement controls.

The model is fully parallelized utilizing the MPI, enabling scalable simulations on HPC environments to efficiently process long-term climate and hydrology datasets over large domains. VIC has been widely used in land surface hydrology studies, climate impact assessments, and operational forecasting systems (Hamman et al., 2018; Liang et al., 1994; Maurer et al., 2002).

2.2.1. Model Configuration and Spatial Resolution

We developed a physically based, high-resolution hydrologic model tailored specifically for the state of New Mexico using the VIC model. The motivation behind this effort is to improve our ability to simulate key water balance components, including evapotranspiration, soil moisture, and runoff across different hydroclimatic regions of New Mexico. Given the diverse physiographic and climatic conditions of the state, a distributed hydrologic model like VIC allows for a more detailed representation of hydrologic processes compared to lumped or

conceptual models. This model serves as a critical tool for water resources management, climate impact assessment, and hydrologic forecasting.

The base parameterization was derived from a validated VIC calibration at a 1/8° resolution, which was subsequently downscaled to 1/16° (Yang et al., 2019). To enhance spatial details, we downscaled soil and vegetation parameters to 1/32° (~3.375 km), aligning with the coupled framework's requirements while preserving calibration integrity. The new MF6 model retains the RGTIHM's 201 m-by-201 m grid, with data exchange facilitated by a joint database described in Section 2.4.6.2. The VIC model operates on a daily time step, resolving water and energy balances to capture seasonal and interannual variability. Soil properties, including texture and depth, were sourced from a 2016 high-resolution dataset (Ketchum, 2016). Vegetation parameters, derived from satellite-based land cover, reflect evapotranspiration regimes across ecological zones.

2.2.2. Parameter Downscaling

Objective 1 of this study was to determine an appropriate spatial resolution for statewide hydrologic modeling. In practice, a 1/32° grid was adopted by quartering the previously validated VIC calibration at 1/16°, which itself had been derived from an earlier 1/8° calibration. This approach preserved the structure of the established calibration while providing finer spatial detail necessary for statewide drought vulnerability analysis. The VIC model requires detailed soil and vegetation parameter datasets, including 53 soil-related parameters distributed across three soil layers as well as vegetation inputs such as the vegetation library and Leaf Area Index (LAI). Downscaling these inputs from 1/16° to 1/32° ensured compatibility with available climate forcings, and supported integration with the coupled computational feasibility for century-scale simulations. While future work should explore alternative resolutions through systematic sensitivity experiments, the 1/32° resolution adopted here provides a practical and defensible baseline for statewide hydrologic modeling. Moreover, the framework supports independent calibration at this finer scale, ensuring that downscaling preserves hydrologic realism rather than relying solely on parameter inheritance from coarser grids.

To achieve the desired resolution, we tested multiple interpolation methods using GRASS, which is a powerful computational engine for raster, vector, and geospatial processing (GRASS Development Team et al., 2025). Nine interpolation methods were considered, with trials

performed to assess their effectiveness. After evaluating the results, we selected v.surf.rst as the preferred interpolation method for downscaling. This method provided the most stable and spatially consistent results, ensuring a smooth transition between spatial scales without introducing artifacts. The downscaling process was conducted using GRASS and shell scripting, automating the resampling workflow for all parameters. The interpolation process included the following steps:

1. Set the computational region to align with the target grid resolution,
2. Perform interpolation of soil parameters using v.surf.rst,
3. Extract interpolated raster values at grid cell centers, and
4. Generate and export the finalized raster dataset.

Through this process, we successfully downscaled the soil and vegetation parameter datasets while preserving the original VIC calibration integrity. This refinement enhances the model's ability to resolve local-scale hydrologic processes while preserving the spatial patterns and values of the original calibrated VIC parameterization.

2.2.3. Meteorological Forcing Data

For this study, we compiled a high-resolution, long-term meteorological forcing dataset spanning from 1991 to 2024 at a daily time step. The data sources and preprocessing steps are as follows:

1. Precipitation was derived from the Parameter-elevation Regressions on Independent Slopes Model (PRISM) Climate Group dataset (PRISM Climate Group, 2026), ensuring high accuracy in spatial and temporal variability.
2. Minimum and maximum temperatures were also sourced from the PRISM, providing continuous and quality-controlled temperature fields.
3. Shortwave and longwave radiation were not directly available, so they were estimated using the Mountain Microclimate Simulation Model (MTCLIM) (Hungerford et al., 1989)—a widely used radiation estimation approach in land surface modeling.
4. Wind speed was obtained from the Gridded Surface Meteorological (gridMET) dataset (Abatzoglou, 2013), which offers high-resolution, gridded wind speed data suitable for VIC applications.

5. Vapor pressure was required by the VIC model as part of the meteorological forcings and added by the MTCLIM.
6. Surface pressure was calculated using the standard atmospheric pressure equation from the US Standard Atmosphere (NOAA, 1976) incorporating elevation-dependent adjustments for improved accuracy.

The equation for the surface pressure in step 6 is defined as:

$$P = P_b \left(1 - \frac{L_b h}{T_b}\right)^{\frac{g_o M_o}{R L_b}} \quad (1)$$

where h is the elevation (m), P is the pressure (hPa) at elevation h, P_b is the reference pressure at sea level (1013.25 hPa), L_b is the assumed constant lapse rate (6°C/km), T_b is the base temperature (K), g_0 is the standard gravitational acceleration (9.81 m/s^2), M_0 is the molar mass of Earth's air (0.029 kg/mol), and R is the universal gas constant (8.31 J/mol/K).

All meteorological forcings were originally at a 4-km resolution and were spatially processed using GRASS and shell scripting to ensure alignment with our VIC grid resolution of 3.375 km (projected resolution of 1/32°). We applied a weighted averaging approach to resample and adjust these datasets to our VIC model domain, ensuring that the atmospheric forcings accurately corresponded to the hydrologic grid. The final preprocessed meteorological data were then read into ESRI's Shapefile format and reformatted into VIC-compatible input files.

This data preprocessing workflow ensures that our VIC model has high-quality forcing inputs, enabling reliable simulation of hydrologic processes across New Mexico. By leveraging advanced geospatial tools and scripting automation, we efficiently handled large datasets and ensured methodological consistency in meteorological data preparation.

2.3. Projected Climate Modeling

To assess future water availability under dynamic climate conditions, we used model data from the CMIP6. We explored multiple datasets from different modeling centers, ensemble members, and downscaling approaches. After comparative evaluation, we selected the MPI-ESM1.2-HR model (Gutjahr et al., 2019). This model provides high-resolution outputs with improved representation of atmospheric and oceanic processes, making it well-suited for hydrologic impact analysis over complex terrains such as New Mexico.

We adopted the Shared Socio-economic Pathways (SSP) SSP5-8.5 scenario, a high-emissions pathway that represents a fossil-fueled development trajectory with limited climate mitigation. This scenario was chosen to capture the upper bound of climate-driven hydrologic stress and assess system vulnerability under extreme warming conditions. Daily climate variables including precipitation, minimum and maximum temperatures, wind speed, shortwave radiation, and longwave radiation were extracted from the MPI-ESM1.2-HR output and processed for the period extending through 2100. While a full uncertainty analysis across climate scenarios was originally planned in Objective 4, this report focuses on projections under the most severe CMIP6 scenario, providing a conservative estimate of future vulnerability.

To integrate the CMIP6 projections with the VIC model domain, we developed a preprocessing workflow in GRASS for spatial extraction, temporal formatting, and preparation of climate inputs for future hydrologic simulations. The raw climate outputs were restructured into VIC-compatible meteorological forcing files. This conversion was completed for the entire simulation period, and the future forcing datasets were fully integrated with the VIC model. The resulting dataset enables physically based simulations of long-term water balance trends and climate-driven hydrologic shifts across New Mexico.

The RGTIHM MF6 model was also extended through 2100 by applying a constant future pumping rate equal to the historical median increased by 10%, based on projected regional population growth (capped at 7% and rounded to the nearest tenth), resulting in a total simulation period spanning 1940 to 2100 (161 years). The 10% pumping increase was applied as a simplified long-term stress scenario rather than as a detailed municipal demand forecast. The scenario uses a conservative 40-year equivalent population growth perturbation of 20.71%, corresponding to an annual growth rate of only 0.472%/yr from 2025 to 2065 (City of Las Cruces, 2017). Because the City of Las Cruces water plan assumes declining per-capita water use through conservation, efficiency improvements, and reduced non-revenue water, pumping demand was not assumed to increase one-to-one with population. Using the low-growth population and demand projections in the water plan, the estimated population-to-pumping response factor is 0.423. Applying this factor to the conservative 40-year population-growth perturbation gives a pumping increase of 8.76%. These supports using a rounded 10% increase as a reasonable and conservative proof-of-concept pumping stress in the MODFLOW extrapolated simulation.

2.4. Framework Architecture

This section describes the methods used to accomplish:

- Objective 2 (Sections 2.4.1–2.4.6): the development of a computationally feasible coupled surface–subsurface hydrologic model, and
- Objective 3: the implementation of distributed computing techniques for large-scale optimization.

2.4.1. Modular Design for Hydrologic Modeling

To address the complexity of statewide hydrologic modeling and ensure reproducibility, we designed a modular framework architecture that integrates geospatial preprocessing, parameter handling, model configuration, simulation execution, and postprocessing into a streamlined computational pipeline. The architecture supports automation at every stage of the VIC and MF6 modeling processes, aiming to minimize manual intervention while maximizing efficiency and transparency. Built entirely on open-source technologies including GRASS, Portable Operating System Interface (POSIX) (IEEE, 2024)-compliant Bash scripts, and C programs, the framework ensures flexibility, accessibility, and interoperability for researchers and practitioners. This modular approach breaks down the modeling process into distinct, interlinked stages, each with a specific functional role, allowing for seamless data flow and consistent execution across large spatial domains and extended temporal periods.

2.4.2. GRASS-Based Spatial Preprocessing

At the heart of the framework lies a robust geospatial preprocessing stage, powered by GRASS as the core engine for spatial data management and transformation. This stage focuses on handling diverse datasets such as land cover, soil properties, vegetation characteristics, and meteorological grids, ensuring they are spatially aligned and formatted for hydrologic modeling. GRASS facilitates critical operations such as raster–vector conversion to harmonize data types, geospatial masking to isolate areas of interest, and spatial interpolation to refine coarse datasets to finer resolutions. For example, interpolation techniques such as v.surf.rst are used to downscale soil and vegetation parameters, ensuring compatibility with VIC's resolution requirements and alignment with MF6 grid cells. The GRASS environment also serves as the spatial backbone, setting consistent gridded computational region boundaries and extracting hydrologic attributes such as soil moisture capacity and runoff potential. All spatial operations

are conducted within project-specific GRASS projects and mapsets (GRASS' terminology for map sets), providing an organized structure for managing data layers and ensuring reproducibility of geospatial workflows across different modeling scenarios.

2.4.3. Workflow Pipeline with Shell Scripting and C Programs

The orchestration of the modeling pipeline is achieved through a suite of modular, POSIX-compliant Bash scripts that automate and sequence the workflow across preprocessing, simulation, and output analysis stages. These scripts act as the glue between different components, managing the execution of GRASS operations, organizing file systems, setting environment variables for computing processes, and coordinating the order in which VIC and MF6 simulations are performed. The scripting layer ensures that each modeling step—ranging from input file preparation and time-step-specific execution to organized output management—is performed reproducibly and without manual intervention. This automation not only reduces the risk of human errors, but also simplifies debugging, supports batch processing, and enables scalability to large spatial domains and multi-decadal temporal windows. By providing a structured approach to workflow management, the scripts create a seamless and efficient environment that can handle the computational demands of statewide hydrologic modeling.

To bridge the gap between geospatial preprocessing and model simulation, we developed a set of C programs optimized for speed and memory efficiency. These programs focus on translating the processed outputs from GRASS into VIC-compatible formats, ensuring that the spatially refined data are preserved and correctly structured for simulation. Specifically, the C programs convert text-based interpolated values into binary VIC parameter files, including datasets for soil properties, vegetation characteristics, and time series data. Given VIC's strict requirements for file formats and efficient I/O handling, the use of compiled C programs significantly reduces the time required for preprocessing large-scale datasets, making the framework suitable for HPC environments. This translation layer ensures that the geospatial data are seamlessly integrated with the VIC simulation engine, maintaining data integrity and computational efficiency throughout the modeling process.

2.4.4. VIC Classic to Image Driver Migration

VIC supports two different model configurations: (1) Classic based on text input files and (2) Image based on NetCDF input files. Each model configuration is simulated by its

corresponding VIC driver. Our model was initially downscaled from the CONUS VIC Classic model by Yang et al. (2019), which follows the time-over-space approach. In this approach, the model simulates all the time steps for a single cell before moving to the next cell. This sequential processing makes the VIC Classic Driver unsuitable for coupled modeling applications, where time-wise synchronicity between surface-water and groundwater processes is important. Coupled modeling requires the space-over-time approach, which processes all grid cells for a single time step before advancing to the next time step. The VIC Image Driver supports the space-over-time approach, making it essential for dynamic coupling with MF6. This limitation of the VIC Classic Driver necessitated migration to the VIC Image Driver, which features a fundamentally different HDF5-based structure compared to the text-based VIC Classic Driver.

2.4.5. MF-OWHM to MF6 Conversion

To extend the framework's capability to groundwater modeling while ensuring a reproducible foundation for the subsequent coupling with VIC, we implemented a Python-based conversion of the RGTIHM from its original MF-OWHM implementation to MF6. This standalone conversion was essential, as the coupling framework relies on a consistent and reproducible MF6 model to integrate groundwater dynamics with VIC's surface water processes effectively. Leveraging the FloPy package for model construction and management, the conversion process was designed to preserve the hydrologic integrity of the original model without altering any input data, ensuring fidelity to the source while adapting to MF6's modern architecture, which offers improved numerical stability and flexibility. The methodology involved initializing a new MF6 simulation with a designated workspace and model name, followed by configuring key packages such as Temporal Discretization (TDIS), Structured Discretization (DIS), Output Control (OC), Iterative Model Solution (IMS), Initial Conditions (IC), and Well (WEL). A sample cross section of the model is illustrated in Figure 2. The Python script utilized additional libraries, including NumPy for array operations, Matplotlib for diagnostic plotting, and GeoPandas for grid export to GeoPackage formats. The DIS package adaptation addressed key differences between MF-OWHM and MF6, converting coordinate origins from upper-left to lower-left, and importing elevation data from text files. Parallel processing using Python's multiprocessing module (with cpu_count) was employed to enhance performance during data processing, with rasterio and contextily supporting spatial data handling and basemap integration for visualization. This Python-driven approach ensured a systematic and

reproducible translation, laying the groundwork for seamless integration of groundwater dynamics with surface water processes modeled by VIC.

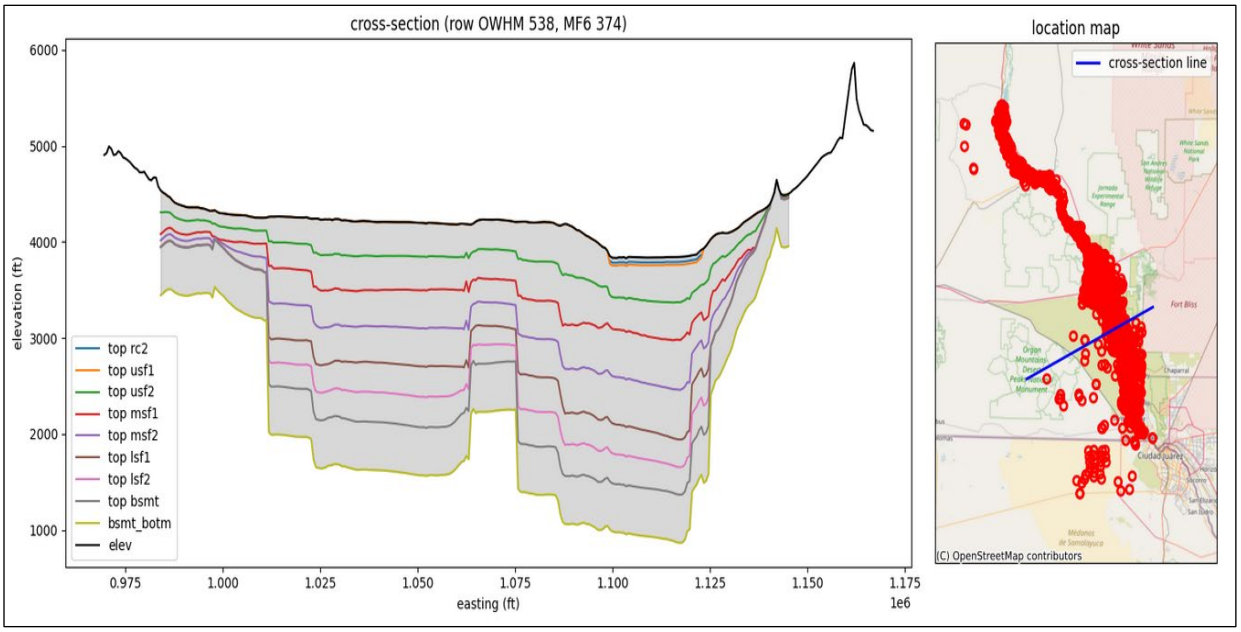

Figure 2. Sample Cross Section of the RGTIHM MF6 Model.

The MF-OWHM to MF6 conversion preserved the core groundwater-flow framework and major hydrologic boundary conditions but did not reproduce all water-management and agricultural-process capabilities available in MF-OWHM. In particular, several MF-OWHM packages, including FMP, HOB, PVL, RES, and ZONE, were not available in MF6 and were therefore omitted or replaced with alternative MF6 functionality where feasible. Because the primary objective of this study was to establish and demonstrate the VIC-MF6 coupling framework, full replication of all MF-OWHM capabilities was beyond the scope of the project. Future work will focus on incorporating additional MF6 packages and agricultural-process functionality to improve consistency with the original RGTIHM implementation.

2.4.6. Coupled Simulation Framework

The VIC-MF6 coupled framework integrates the VIC model with MF6 to simulate dynamic interactions between surface-water and groundwater systems through the exchange of key hydrologic fluxes across the land surface–groundwater interface. The framework combines VIC simulations for the periods 1990–2024 (historical) and 2025–2100 (projected) with MF6 simulations for 1940–2014 (historical) and 2015–2100 (projected based on a constant pumping

rate equal to 110% of the historical median pumping rate), enabling integrated simulations spanning 1940–2100. The name VIC-MF6 reflects the use of MF6 as the groundwater modeling component and its API- and XMI-based coupling capabilities, which facilitate integration with VIC in ways that were not possible with earlier MODFLOW versions.

The hydrologic methodology centers on the Unsaturated Zone Flow (UZF) package within MF6, which facilitates the bidirectional transfer of water. VIC generates baseflow (out_baseflow), representing the infiltration from surface processes, which is translated into infiltration (finf) for MF6's UZF package. This flux is adjusted using area-weighted ratios to account for differences in spatial resolution between the models. In return, MF6 calculates groundwater discharge to the land surface (gwd) via the UZF package, which influences VIC's soil moisture dynamics. The gwd is incorporated into VIC's initial moisture (init_moist) parameter for the third soil layer when positive, reflecting groundwater contributions to surface conditions; if gwd is zero, init_moist is set to zero. This approach ensures a physically consistent representation of water movement, capturing feedback mechanisms critical for simulating integrated hydrologic processes over extended temporal scales, such as the 161-year period from 1940 to 2100. The coupling region is defined by the spatial extent of the MF6 groundwater model domain, where VIC and MF6 exchange hydrologic fluxes, including recharge and groundwater discharge, to represent surface–subsurface interactions. Outside this domain, hydrologic processes are simulated using VIC alone because no groundwater model is available for coupling.

2.4.6.1. Hydrological Exchange. The exchange loop, managed by the CouplingManager class, orchestrates the monthly coupling between VIC and MF6, aligning their simulations to reflect integrated hydrologic dynamics. The process begins with VIC and MF6 running a monthly stress period, producing three key outputs: two from VIC—a state file for pausing and resuming the surface simulation and a water balance (wbal) file containing out_baseflow—and one from MF6—the UZF package's groundwater discharge (gwd). If gwd exceeds zero, it is area-weighted for VIC grid cells and used to update VIC's init_moist parameter in the parameter file (nc5_params.nc) for the next iteration. Otherwise, init_moist is set to zero and the wbal file is read using the netCDF4 library to extract the baseflow data, which is then converted into finf for MF6's UZF package. The finf variable is computed by weighting the baseflow with area ratios derived from the coupling table, ensuring resolution differences are addressed. Both VIC and

MF6 then simulate the same monthly period and repeat the same iteration until the end of the coupling period. This loop iterates monthly, with each cycle logging the exchanged fluxes (finf, gwd) and updated init_moist values to a Comma-Separated Values (CSV) file, ensuring traceability. The process continues from VIC's start date (January 1, 1990) to the coupling end date (December 31, 2100), with MF6 initialized from its manual start date (March 1, 1940) to just before VIC begins.

2.4.6.2. Spatial Connectivity for the Exchange. The spatial exchange is supported by a joint table generated through a shell script leveraging GRASS, which creates a coupling database matching the VIC and MF6 UZF region cells. This script intersects the VIC and MF6 cell layers to identify overlapping areas, and computes intersection areas and area ratios. VIC cells are assigned integer IDs (vic_id), while MF6 cells use a six-digit padded string format (mf6_id) based on row and column indices. The resulting mf6_vic_join table includes columns for vic_id, mf6_id, a unique coupling ID (cpl_id), intersection area (area_m2), and area ratios (mf6_area_ratio and vic_area_ratio), with the last two columns calculated as the intersection area divided by the MF6 cell area and VIC cell area, respectively. This table is exported as a CSV file with the six columns (vic_id, mf6_id, cpl_id, area_m2, vic_area_ratio, and mf6_area_ratio), providing a weighted average mechanism to exchange variables such as baseflow and gwd across differing resolutions, ensuring accurate flux distribution during the coupling process.

2.4.6.3. Implementation with the MF6 API. The MF6 API, foundational to this framework, is built upon the Basic Model Interface (BMI) standard (Hutton et al., 2020), extended by the XMI, as outlined by Hughes et al. (2022):

> "To facilitate coupling with other models, including those written in different languages, an Application Programming Interface (API) was developed for MODFLOW, leveraging the BMI standard established by the Community Surface Dynamics Modeling System (CSDMS) to provide a component-based interface for Earth-science models. This choice was informed by other coupling standards such as the Common Component Architecture, the Earth System Modeling Framework, and the Open Modeling Interface, with BMI selected for its specific design for Earth-science applications and its clear applicability to coupling MODFLOW with community-relevant process models."

Our coupling framework's highly modularized structure utilizes custom classes and functions, with the mf6.Model class initializing the model via xmipy.XmiWrapper to access the MF6 API, parsing grid and time discretization data (nlay, nrow, ncol, nper, and nstp) through XMI methods, and managing UZF variables (finf and gwd) for data exchange. The VICModel class handles VIC execution, updating the global parameter file dynamically with shutil and subprocess calls, and processing NetCDF outputs with the netCDF4 library. The CouplingManager class serves as the orchestrator, utilizing the pandas package to manage the coupling table and the NumPy package to perform array operations, implementing the exchange logic with weighted averaging based on the joint table. Figure 3 provides an overview of the coupling flowchart implemented in the framework.

The framework's modularity allows independent testing and scaling, with error handling and logging via the logging module ensuring robustness. This design, grounded in the XMI-based MF6 API, facilitates HPC compatibility and seamless integration of VIC and MF6, supporting the framework's scalability for statewide hydrologic modeling.

2.4.7. Development of Parallel Optimization Techniques for Large-Scale Hydrologic Modeling

Under Objective 3, the originally sequential Isolated-Speciation-Based Particle Swarm Optimization (ISPSO) (Cho et al., 2011) was developed into Parallel ISPSO using resources from this project. Parallel ISPSO is a general-purpose parallel optimization algorithm designed to evaluate efficiently large numbers of candidate solutions across distributed computing nodes in HPC environments, making it suitable for high-dimensional, large-scale hydrologic model optimization. The original ISPSO algorithm was implemented in R, and its parallelization was built using the parallel library. Specifically, the makeCluster, clusterExport, clusterApply, and stopCluster functions enable the distribution of workloads across multiple machines over a network and the collection of model run results for parallel optimization.

While Parallel ISPSO was successfully developed, its application to the VIC-MF6 coupled hydrologic model was not feasible because the MF6 domain's complex fault structures limited opportunities for efficient model decomposition and load-balanced parallelization. However, it is worth noting that the coupled VIC-MF6 framework was applied to already calibrated models, mitigating the immediate need for large-scale optimization within the current project scope.

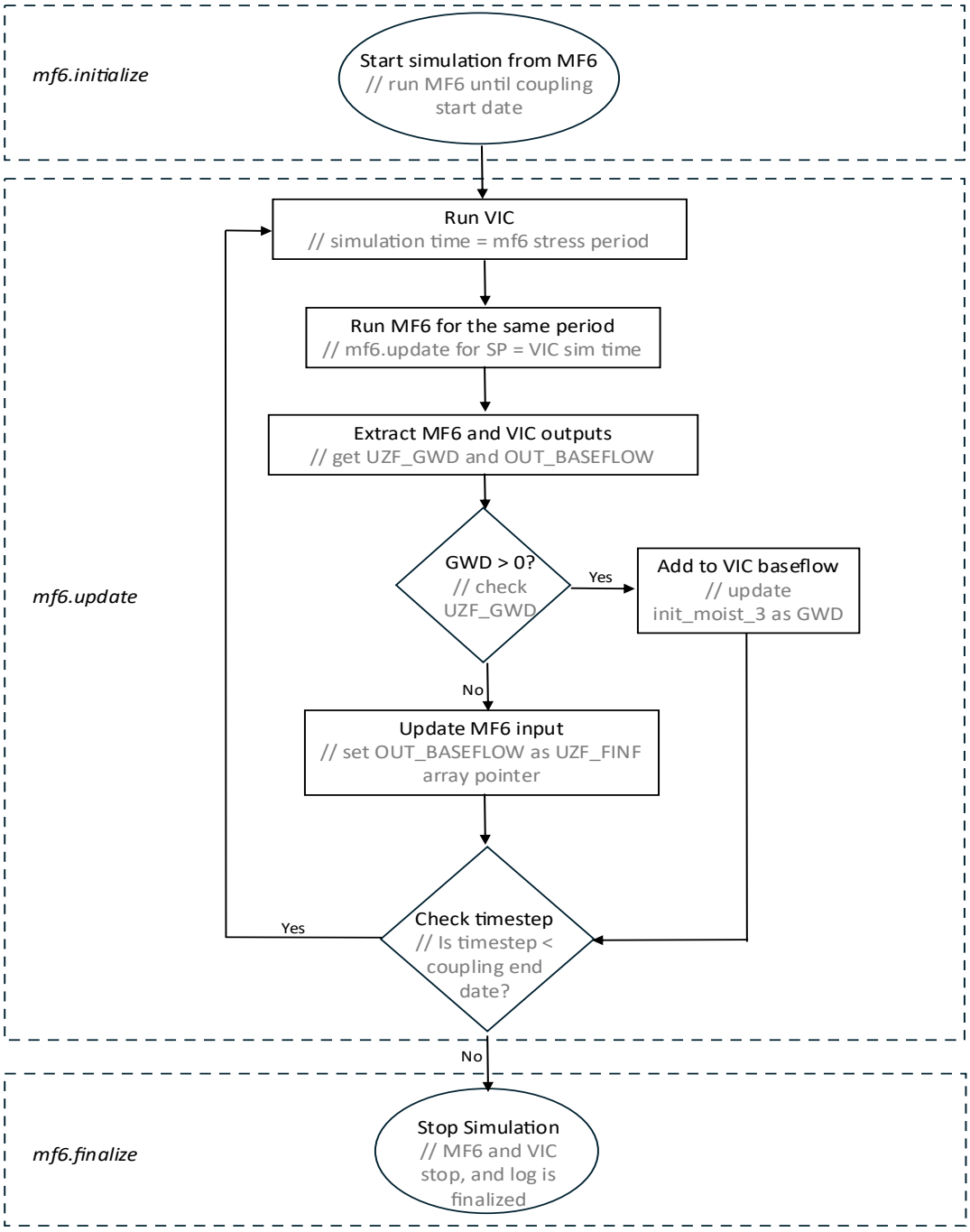

Figure 3. Flowchart of the VIC-MF6 Coupling Framework Using the MF6 API's mf6 Routines (mf6-driven control).

The efficiency and functionality of this new parallel optimization algorithm were demonstrated through separate SWAT model optimization runs. This demonstration used independent resources and serves to validate Parallel ISPSO's potential for large-scale VIC-MF6 hydrologic model applications. The development of Parallel ISPSO under this project represents

a technical contribution and provides a foundation for future optimization efforts across diverse modeling frameworks. Future work could explore Parallel ISPSO to further accelerate parameter estimation and optimization in fully decomposable large-scale hydrologic models.

2.5. Drought Vulnerability Analysis

This section describes the methods used to calculate a statewide DVI to inform water resources management (Objective 5).

2.5.1. Rationale and Design Choices

A hydrology-driven indicator framework was implemented to map drought vulnerability at monthly resolution. The design follows the hazard-sensitivity-exposure structure typically used in vulnerability mapping (Carrão et al., 2016; Naumann et al., 2014). Standardized hydroclimate indices including Standardized Precipitation Index (SPI), Standardized Precipitation-Evapotranspiration Index (SPEI), Standardized Runoff Index (SRI), Standardized Soil Moisture Index (SSI), and Standardized Snow Drought Index (SDI) were used to represent concurrent meteorological, soil moisture, runoff, and snow anomalies (McKee et al., 1993; Shukla and Wood, 2008; Vicente-Serrano et al., 2010). Month-wise, nonparametric standardization was chosen to avoid parametric fit errors under skewed and zero-inflated conditions (Farahmand and AghaKouchak, 2015).

A fixed baseline of 1990–2009 was used for all "training" steps. Here, "training" refers to computing all baseline statistics (month-wise empirical Cumulative Distribution Functions [CDFs] for rank-to-z mapping, min-max scaling bounds, and monthly climatic indicators used in exposure) from 1990–2009 only and applying these fixed mappings to the entire 1990–2100 period; no parameters are estimated from data after 2009. A fixed baseline prevents temporal leakage and keeps indices comparable over time; therefore, a 20-year baseline provides 20 samples for each calendar month. This baseline length is adequate for rank-based, nonparametric mapping to a standard normal score and is common when the recent climate is the reference of interest (Farahmand and AghaKouchak, 2015). Thirty-year normals are conventional in climatology (Arguez and Vose, 2011), but the 20-year choice was made to emphasize recent hydroclimate conditions while maintaining sufficient samples. A 12-month backward window was used for hydrological drought metrics. This window integrates multi-season anomalies and catchment memory. Studies report that 6- to 12-month time scales correlate well with storage and

streamflow deficits. A 12-month window is a common compromise between responsiveness and memory (Bloomfield and Marchant, 2013; Farahmand and AghaKouchak, 2015; Van Loon, 2015; Vicente-Serrano et al., 2010). Figure 4 shows the flowchart for DVI calculation.

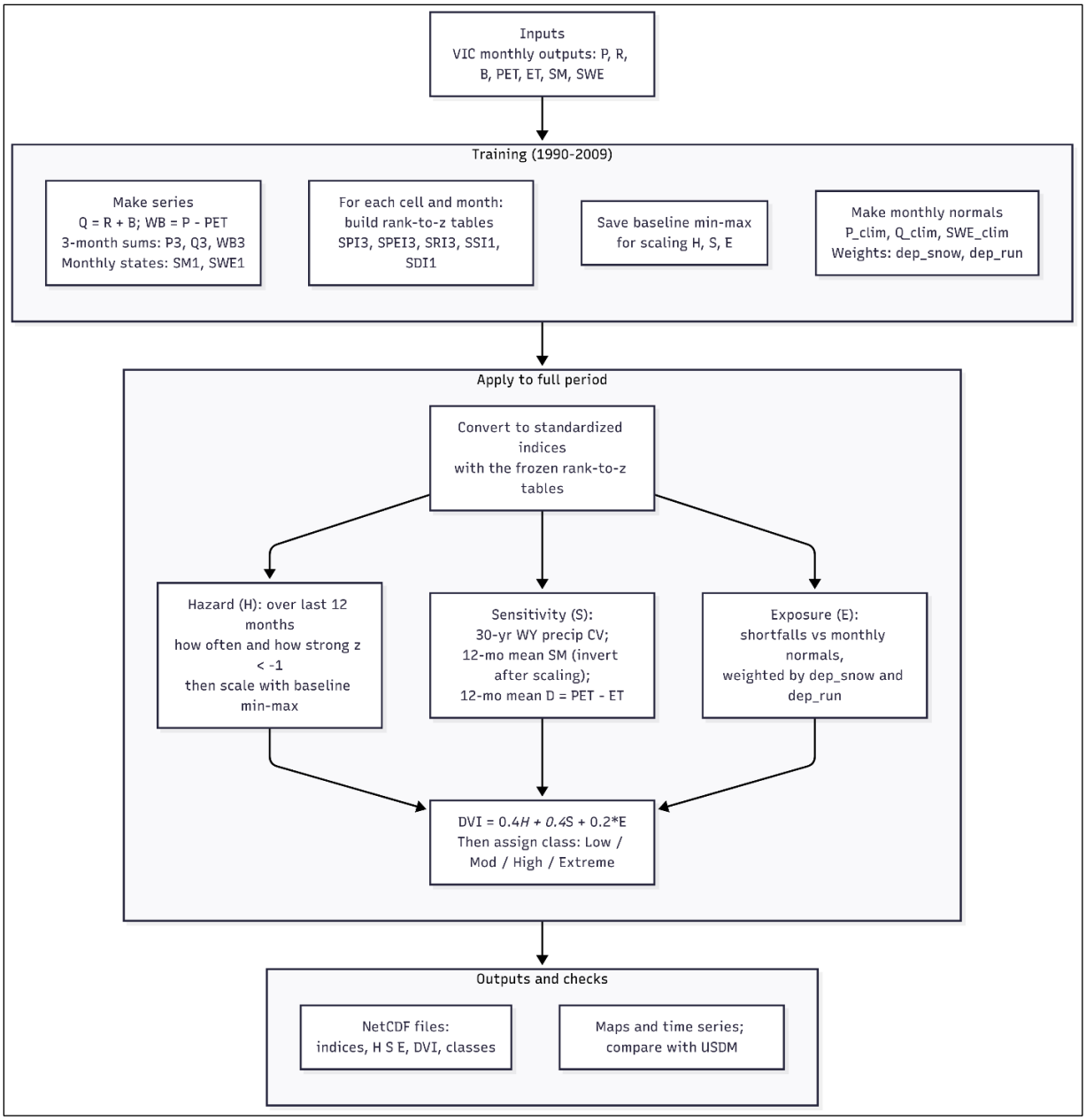

Figure 4. Flowchart for DVI Calculation.

2.5.2. Data and Domain

The drought vulnerability analysis utilized monthly post-processed outputs from the VIC model across New Mexico. The variables included precipitation (P), runoff (R), baseflow (B),

potential evapotranspiration (PET), evapotranspiration (ET), soil moisture (SM, end of month), and snow water equivalent (SWE, end of month). The first five variables are water balance flux outputs and averaged monthly, while the last two are state variables at the end of each month. All spatial coordinates were represented in the geographic coordinate system, specifically the European Petroleum Survey Group (EPSG) code EPSG:4326, and a static land mask was applied to define the model domain consistently.

Temporal data were recorded at monthly intervals and were decoded to a consistent calendar. All standardizations and min-max scalings used for computing the DVI were derived from the 1990–2009 baseline period and applied unchanged to the entire historical and projected dataset for 1990–2100, ensuring comparability and consistency in relative drought assessments across the full temporal domain. This output dataset combines statewide VIC simulations with coupled surface–subsurface simulations in the Lowr Rio Grande Basin, providing the spatially and temporally continuous hydrologic information required for drought vulnerability assessment.

2.5.3. Stage 1: Baseline-Fixed Standardization of Hydrologic Indices

Two derived fluxes were formed:

$$Q = R + B \quad \text{(total runoff)}, \qquad \mathrm{WB} = P - \mathrm{PET} \quad \text{(water balance)}.$$

Short-term horizons were represented by 3-month accumulations for fluxes (P_3, Q_3, WB_3) and 1-month states (SM_1, SWE_1):

$$P_3 = \sum_{k=0}^{2} P_{t-k}\,, \quad Q_3 = \sum_{k=0}^{2} Q_{t-k}\,, \quad \mathrm{WB}_3 = \sum_{k=0}^{2} \mathrm{WB}_{t-k}\,, \quad \mathrm{SM}_1 = \mathrm{SM}_t, \quad \mathrm{SWE}_1 = SW\mathrm{E}_t$$

where t is the current month. For each grid cell and calendar month t, baseline values were used to compute empirical percentiles p for $A \in \{P_3, Q_3, \mathrm{WB}_3, \mathrm{SM}_1, \mathrm{SWE}_1\}$:

$$p = \frac{\mathrm{rank}(A) - 0.5}{n}, \quad n = 20$$

where n is the number of baseline years. Percentiles were clipped to $[10^{-4},\ 1 - 10^{-4}]$ and mapped to standard normal scores $z = \Phi^{-1}(p)$, where $\Phi(\cdot)$ indicates the CDF of a normal distribution. The z scores were used to define the following standardized indices:

$$\mathrm{SPI}_3 \leftarrow P_3, \quad \mathrm{SRI}_3 \leftarrow Q_3, \quad \mathrm{SPEI}_3 \leftarrow WB_3, \quad \mathrm{SSI}_1 \leftarrow SM_1, \quad \mathrm{SDI}_1 \leftarrow SWE_1$$

where lower index values indicate drier conditions. We considered index values below -1 as an indicator for droughts.

2.5.4. Stage 2: Vulnerability Components

2.5.4.1. Hazard. At each time t, breadth b_t—the fraction of indices below -1 (drought conditions)—was computed using the following equation:

$$b_t = \frac{1}{5}\sum_{X} \chi_{(-\infty,-1)}(X_t)$$

where $X \in \{\mathrm{SPI}_3, \mathrm{SPEI}_3, \mathrm{SSI}_1, \mathrm{SRI}_3, \mathrm{SDI}_1\}$ and $\chi_{(-\infty,-1)}(x)$ is the step function that returns 1 if $x < -1$ and 0 otherwise. Frequency $\mathrm{Freq}_{12}(t)$ and severity $\mathrm{Sev}_{12}(t)$ over a 12-month window were then computed as follows:

$$\mathrm{Freq}_{12}(t) = \frac{1}{12}\sum_{k=0}^{11} b_{t-k}\,, \qquad \mathrm{Sev}_{12}(t) = \frac{1}{12}\sum_{k=0}^{11}\left[\frac{1}{5}\sum_{X} X_{t-k}\chi_{(-\infty,-1)}(X_{t-k})\right],$$

with $\mathrm{Sev}_{12}(t) = 0$ if no drought months occurred in the window. Both metrics were min-max scaled to $[0,1]$ using baseline extrema as $\widehat{x(t)} = \frac{x(t)-x_{baseline,min}}{x_{baseline,max}-x_{baseline,min}}$. The hazard component is defined using the min-max scaling as

$$H_t = \frac{1}{2}\left[\widehat{\mathrm{Freq}}_{12}(t) + \widehat{\mathrm{Sev}}_{12}(t)\right].$$

The first 11 months are undefined by construction.

2.5.4.2. Sensitivity. Three metrics were used. (i) Water-year (October–September) precipitation totals were computed and a rolling 20-year Coefficient of Variation (CV) was formed; the CV was assigned to constituent months and min-max scaled on the baseline. (ii) The 12-month mean soil moisture $\overline{SM}_{12}(t)$ was min-max scaled and then inverted after scaling so that lower buffering implies higher sensitivity. (iii) The 12-month mean evaporative deficit $\overline{D}_{12}(t)$ with $D = \mathrm{PET} - \mathrm{ET}$ was min-max scaled. Sensitivity S_t is the average of the three scaled metrics:

$$S_t = \frac{1}{3}\left[\widehat{\mathrm{CV}}_{P,20}(t) + \left(1 - \widehat{\overline{SM}}_{12}(t)\right) + \widehat{\overline{D}}_{12}(t)\right].$$

Metrics are undefined until the required window length is available.

2.5.4.3. Exposure. Long-term reliance on snow storage and runoff was quantified by

$$\mathrm{dep}_{\mathrm{snow}} = \frac{\overline{\mathrm{SWE}}_{\mathrm{clim}}}{\overline{P}_{\mathrm{clim}} + \varepsilon}, \qquad \mathrm{dep}_{\mathrm{run}} = \frac{\overline{Q}_{\mathrm{clim}}}{\overline{P}_{\mathrm{clim}} + \varepsilon},$$

where $\varepsilon = 10^{-6}$ to avoid a singularity?. Monthly climatologies were computed from 1990–2009 and annual means were taken across months. Monthly shortfalls relative to climatology were

$$\mathrm{swe}_{\mathrm{rel}}(t) = \max\left(0,\, 1 - \frac{\mathrm{SWE}_t}{\mathrm{SWE}_{\mathrm{clim}}(m_t)}\right), \qquad \mathrm{q}_{\mathrm{rel}}(t) = \max\left(0,\, 1 - \frac{Q_t}{Q_{\mathrm{clim}}(m_t)}\right),$$

with m_t the calendar month. The raw unscaled exposure index was

$$E_t^* = \frac{1}{2}\mathrm{dep}_{\mathrm{snow}}\,\mathrm{swe}_{\mathrm{rel}}(t) + \frac{1}{2}\mathrm{dep}_{\mathrm{run}}\,\mathrm{q}_{\mathrm{rel}}(t)$$

and then min-max scaled to $E_t \in [0,1]$. This structure down-weights snow-free areas through small $\mathrm{dep}_{\mathrm{snow}}$ and responds to actual shortfalls where reliance is high.

2.6. Stage 3: Composite DVI and Classes

Components were combined using fixed weights:

$$\mathrm{DVI}_t = 0.4\,H_t + 0.4\,S_t + 0.2\,E_t, \qquad \mathrm{DVI}_t \in [0,1].$$

For maps, four classes were defined: Low $[0,0.25]$, Moderate $[0.25,0.50]$, High $[0.50,0.75]$, and Extreme $[0.75,1]$ (Svoboda et al., 2002).

3. RESULTS AND DISCUSSION

3.1. VIC Classic to Image Program

The transition to VIC Image was successfully achieved across the statewide model using the VIC Classic to Image Converter, a standalone C-based tool developed to streamline VIC model transitions. This converter accepts a VIC Classic global parameter file as its sole argument and transforms the entire model—including meteorological forcing, soil and vegetation parameters, and vegetation library—into the HDF5 NetCDF format required by the VIC Image Driver. For the statewide model, encompassing diverse spatial domains, the converter completed the transformation in under 200 s, showcasing its efficiency and scalability for large-scale applications. Validation checks confirmed that the converted VIC Image Driver model preserved data integrity, with input parameters (e.g., soil properties and meteorological forcing) exhibiting

zero discrepancies compared to the original VIC Classic inputs. This conversion enabled synchronized, space-over-time simulations across all grid cells per time step, fully aligning with MF6's temporal requirements. By eliminating VIC Classic's synchronicity limitations and bypassing RVIC's (an R package for running VIC Classic in parallel) memory constraints discussed in Section 3.3.1, the VIC Classic to Image Converter established a scalable and efficient surface water modeling framework, significantly enhancing the performance and compatibility of the coupled VIC-MF6 system.

3.2. MF-OWHM to MF6 Conversion

The conversion of the RGTIHM from MF-OWHM to MF6 preserved the core groundwater-model framework across the LRG region. Comparative inspection of model inputs confirmed consistency in grid discretization, hydraulic properties, and major boundary conditions between the two implementations as shown in Figure 5. The MF6 model maintained the original domain of 912 rows and 328 columns, with active cell counts ranging from 17,879 in Layer 1 to 112,576 in Layer 9 out of 299,136 total cells, and initial head values spanning 950 ft to 5,476 ft, aligning precisely with MF-OWHM inputs. Diagnostic visualizations, including cross sections and top elevation contours, further validated correct grid orientation and layer alignment, with inactive cell distributions matching expected geological features, establishing a reliable foundation for coupled modeling. The conversion and writing the files in MF6 format takes about 50 min. Because several MF-OWHM-specific packages were not incorporated into MF6, the converted model should be viewed as a preservation of the core hydrogeologic framework rather than a complete functional replication of the original RGTIHM.

3.3. Coupled Surface and Groundwater Framework

The coupled hydrologic modeling framework successfully integrated the VIC model for statewide surface-water processes with the MF6 model for groundwater dynamics in the LRG region, enabling bidirectional surface–subsurface interactions within the LRG groundwater-model domain. This integration provides a coupled representation of water resources in the LRG region from 1990 to 2100 and establishes a framework for future expansion toward a more comprehensive representation of water resources across New Mexico. The implementation was executed using the Python coupling framework and its outputs were postprocessed and visualized using the R programming language. Below, we discuss the performance of parallel

execution, the individual VIC and MF6 results, and the framework's application for drought assessment. The run took about 650 min (almost 11 h) to complete on a single core.

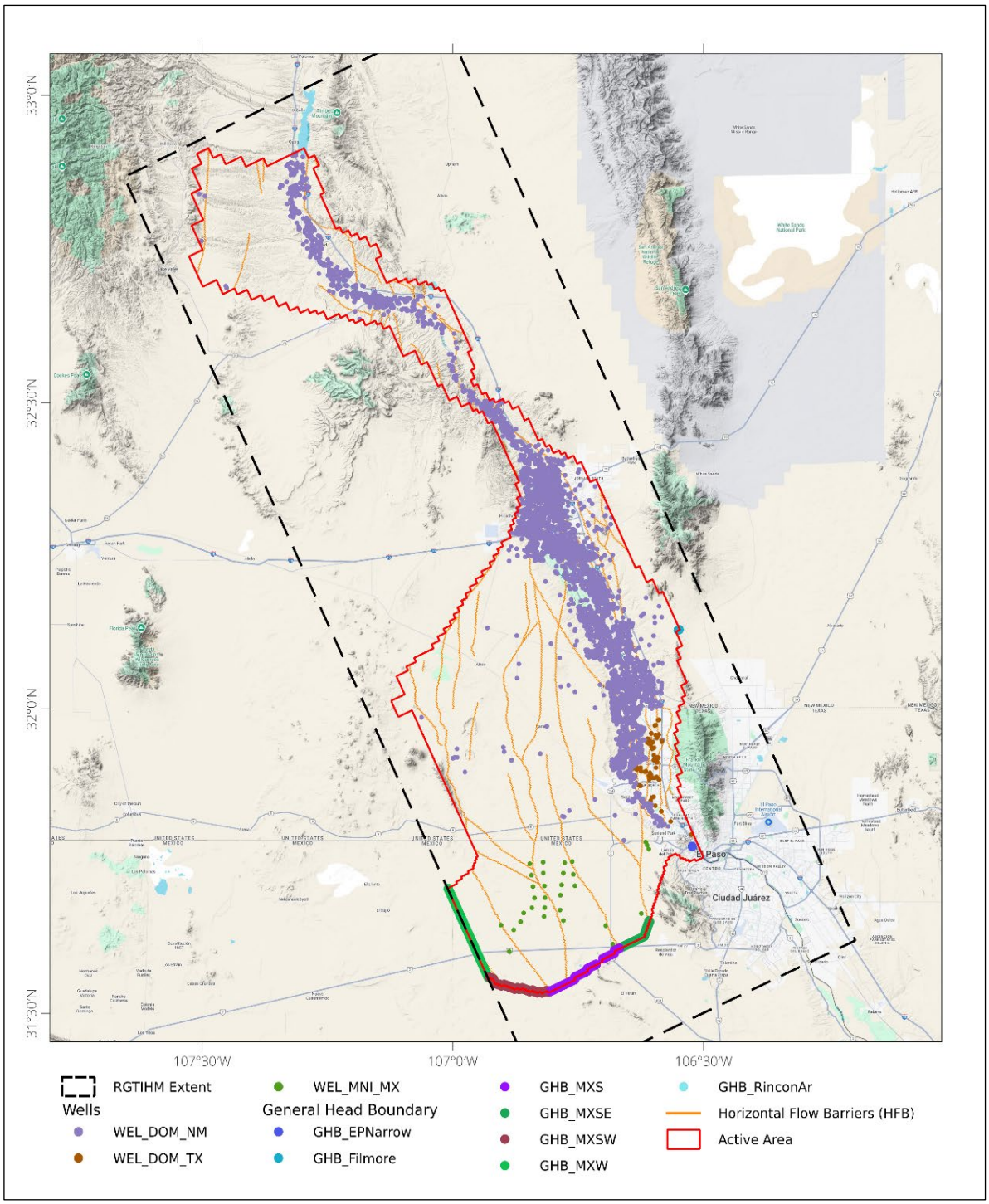

Figure 5. RGTIHM MF6 with General Head Boundary, Wells, and Horizontal Flow Barrier Packages.

Results in this section are presented as a proof-of-concept demonstration of the coupled VIC-MF6 framework. The simulations completed successfully and produced numerically stable, physically plausible hydrologic responses. The interpretations provided in this section are necessarily preliminary because they are based on proof-of-concept simulations and statewide aggregated statistics that do not fully resolve regional variations in climate, topography, snow processes, groundwater conditions, and water management practices. More rigorous calibration, validation, and regional analysis are identified as important future work.

3.3.1. Performance of Parallel VIC and MF6

Parallel execution of both VIC and MF6 models delivered significant performance improvements while preserving simulation accuracy across the LRG Basin. Table 1 summarizes the runtime and efficiency gains for both models under sequential and parallel configurations. For MF6, using six processes (np=6), the runtime was reduced by 59.3% (from 110 min to 45 min). For VIC, parallel execution using the RVIC R library with four processes (np=4) achieved a runtime reduction from 69 min to 24 min, yielding a speedup efficiency of 95.8%. These speedups, achieved without altering model outputs, demonstrate the scalability of both models for large-scale simulations within the VIC-MF6 framework, supporting extended temporal and complex spatial analyses.

Table 1. Parallel Performance of VIC and MF6. The number of processes is given by np.

Model	Runtime (Sequential)	Runtime (Parallel)	Efficiency
MF6	110 min	45 min	40.7% (np=6)
VIC Classic	69 min	24 min	95.8% (np=4)

However, initial testing revealed limitations in the VIC Classic and RVIC setup. VIC Classic's time-over-space approach, processing all time steps for a single cell before moving to the next cell, prevented the temporal synchronicity required for integration with MF6, which demands a space-over-time framework. Additionally, RVIC exhibited memory inefficiencies, duplicating input data for each submodel, leading to excessive memory consumption. Trials at 25%, 50%, 75%, and 100% of the full model size showed that RVIC could not support more than three submodels for the full model or six submodels at a 25% scale, with memory usage scaling

unfavorably as the submodel count increased. These issues were resolved by transitioning to VIC Image, as described earlier.

3.3.2. Surface Water Hydrology

The VIC model provides an assessment of surface water dynamics in New Mexico from 1990 to 2100, with the period from 1990 to 2024 simulated using observed meteorological forcings and 2025 to 2100 based on CMIP6 forecasted data. The analysis focuses on key hydrologic metrics, including runoff, baseflow, and soil moisture, as detailed below.

Figure 6 illustrates monthly runoff trends over the simulation period, with a 12-month moving average depicted in red. During the observed period (1990–2024), runoff exhibits seasonal variability, peaking during the monsoon months of July and August, with the red moving average highlighting a stable trend over time. In the forecasted period (2025–2100), runoff shows increased seasonal peaks, with the moving average suggesting a gradual upward trend, reflecting potential hydrologic responses to projected climate conditions as of August 1, 2025.

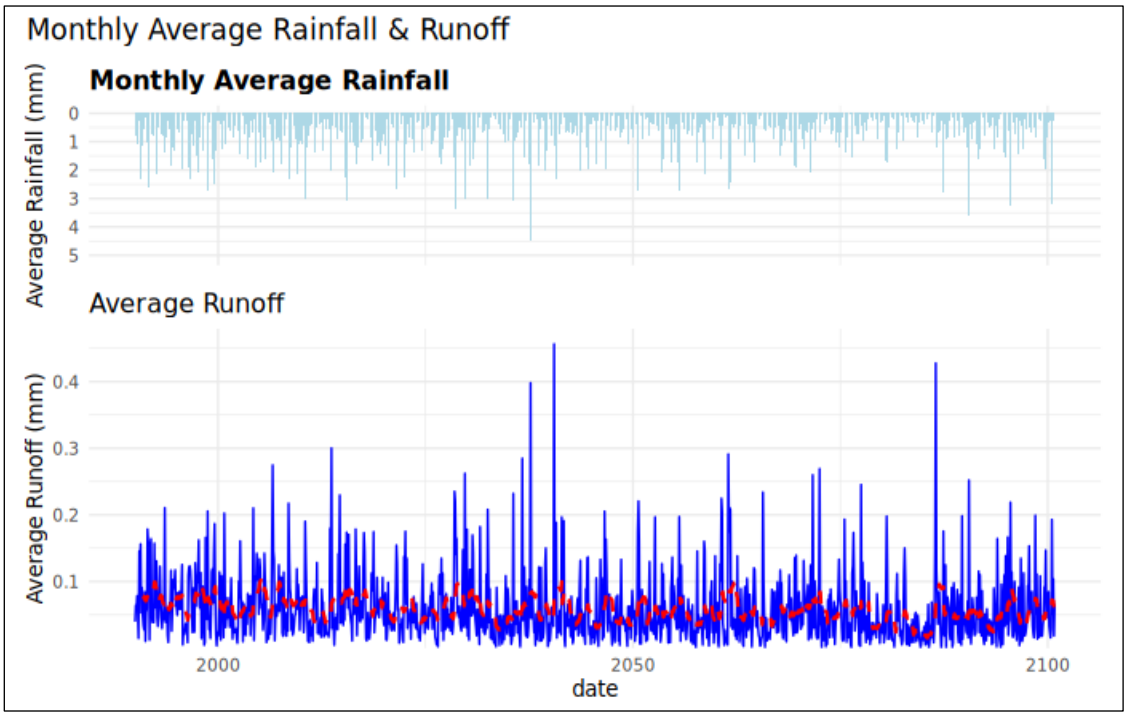

Figure 6. Average Monthly Runoff for the Simulation Period with Monthly 12-Month Moving Average in Red.

Figure 7 details baseflow dynamics. In the observed period, baseflow shows seasonal increases following monsoon rainfall, maintaining a consistent baseline with notable peaks in wet years. The forecasted period indicates a slight rise in baseflow, with sustained elevated levels post-2050, suggesting enhanced groundwater contributions under CMIP6 projections. The sudden peak at the beginning of the forecasted period suggests that the publicly available bias-corrected CMIP6 products sometimes require local bias correction to adjust the data as per the local climatic and hydrologic conditions.

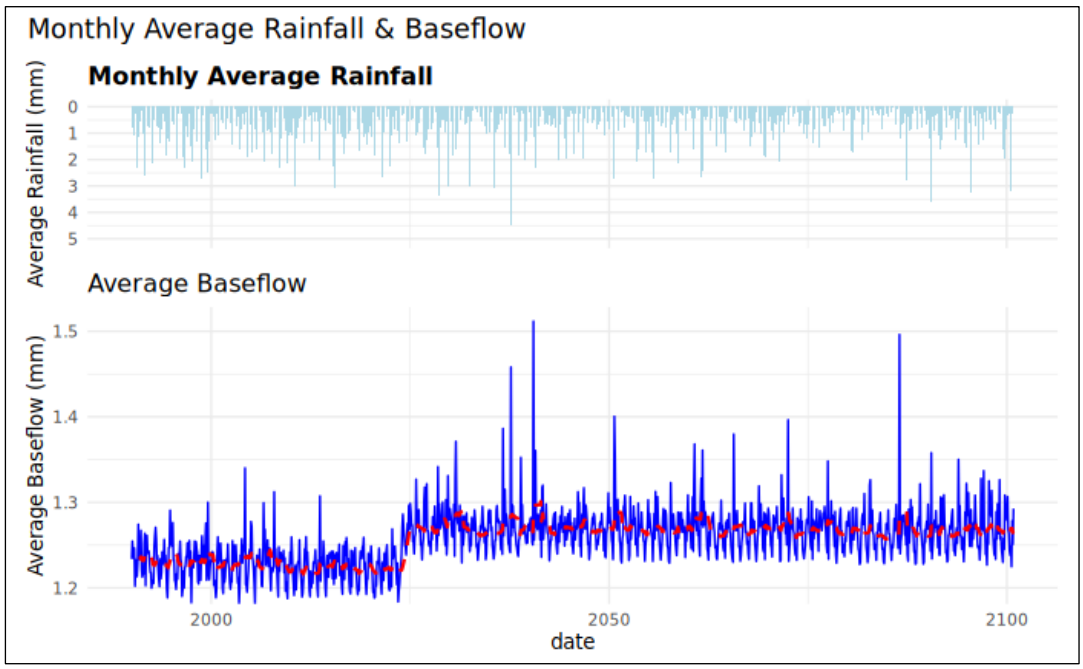

Figure 7. Average Monthly Baseflow for the Simulation Period with Monthly 12-Month Moving Average in Red.

Figure 8 shows strong seasonal variation in monthly precipitation for the entire climatic forcing period 1990–2100. In all boxplots, the central line represents the median, the box bounds represent the first and third quartiles (Q1 and Q3), the whiskers extend to 1.5 times the Interquartile Range (IQR) beyond the quartiles, and points beyond the whiskers are plotted as outliers. Medial rainfall is generally below 1 mm during most months but increases substantially during the summer monsoon season (July–September), ranging from approximately 1.3 to 1.4 mm, when both precipitation amounts and variability are greatest. These months exhibit the widest IQRs of 0.5–2.1 mm in July, 0.7–2.0 mm in August, and 0.8–1.8 mm in September,

indicating more frequent high-precipitation events. In contrast, the remaining months show lower precipitation and relatively narrow distributions.

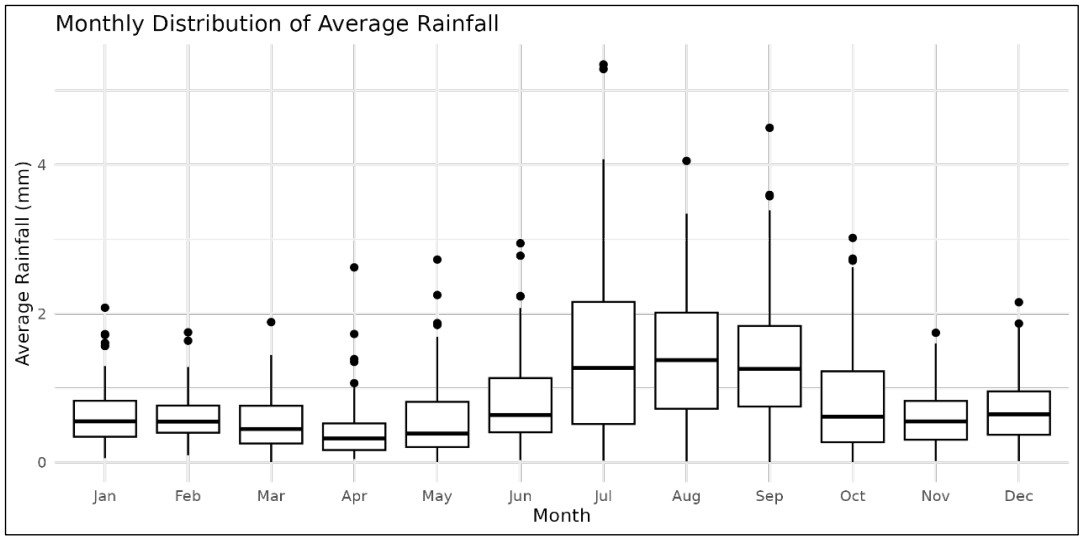

Figure 8. Boxplots of Average Monthly Rainfall.

Figure 9 presents soil moisture trends. During the observed period, soil moisture fluctuates with seasonal rainfall, peaking during the monsoon season and stabilizing in drier months. The forecasted period shows a modest increase in peak soil moisture levels, indicating potential changes in water retention capacity through 2100 under forecasted conditions.

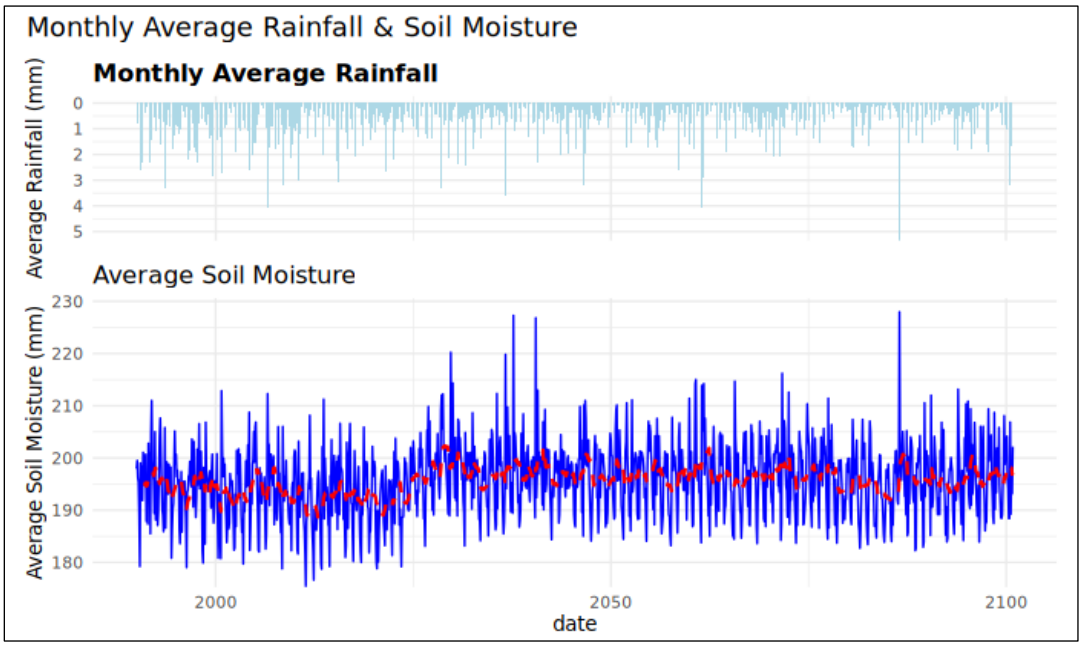

Figure 9. Average Monthly Soil Moisture for the Simulation Period with Monthly 12-Month Moving Average in Red.

Figure 10 illustrates the seasonal variability of runoff across the simulation period. The median of statewide monthly average runoff is approximately 0.05 mm, reflecting moderate monthly variation. Outliers extend up to 0.50 mm, predominantly during the monsoon months of July and August, indicating significant seasonal peaks driven by observed and forecasted precipitation patterns.

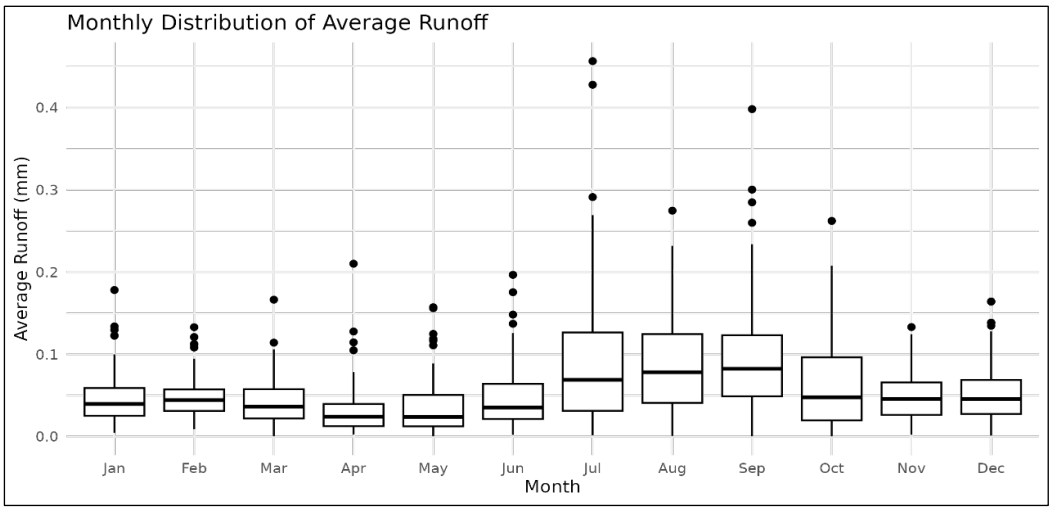

Figure 10. Boxplots of Average Monthly Runoff.

Figure 11 presents the monthly variability of soil moisture. The median soil moisture is 210 mm, with an IQR of 200–220 mm, indicating a consistent baseline across months. Outliers extend to 230 mm during peak monsoon periods, reflecting increased water retention in response to observed rainfall (1990–2023) and forecasted conditions (2024–2100).

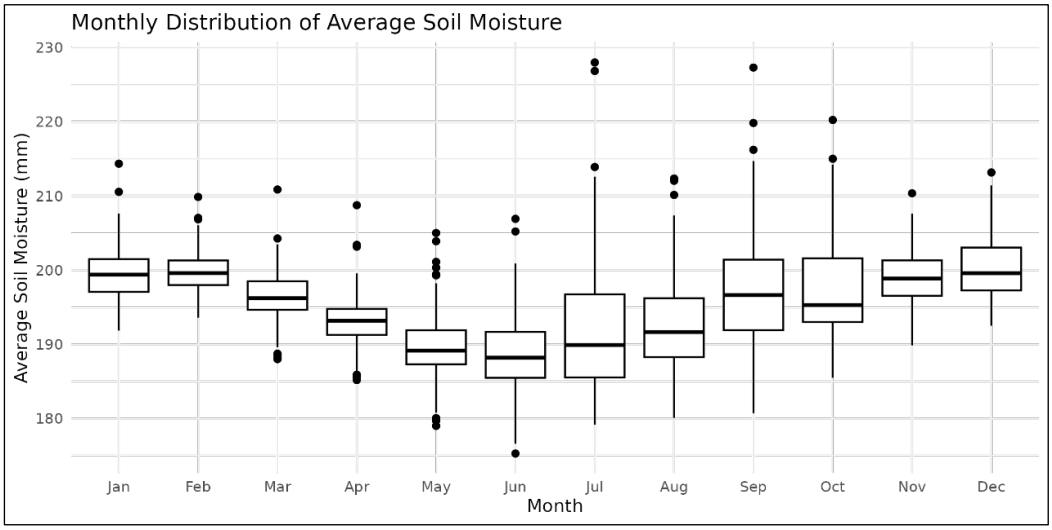

Figure 11. Boxplots of Average Monthly Soil Moisture.

Figure 12 details the monthly dynamics of baseflow. The median baseflow is 1.35 mm, with an IQR of 1.20–1.45 mm, suggesting a stable monthly distribution. Seasonal variations are minimal, with outliers reaching 1.55 mm during wetter months, likely influenced by monsoon recharge and sustained groundwater contributions under CMIP6 projections.

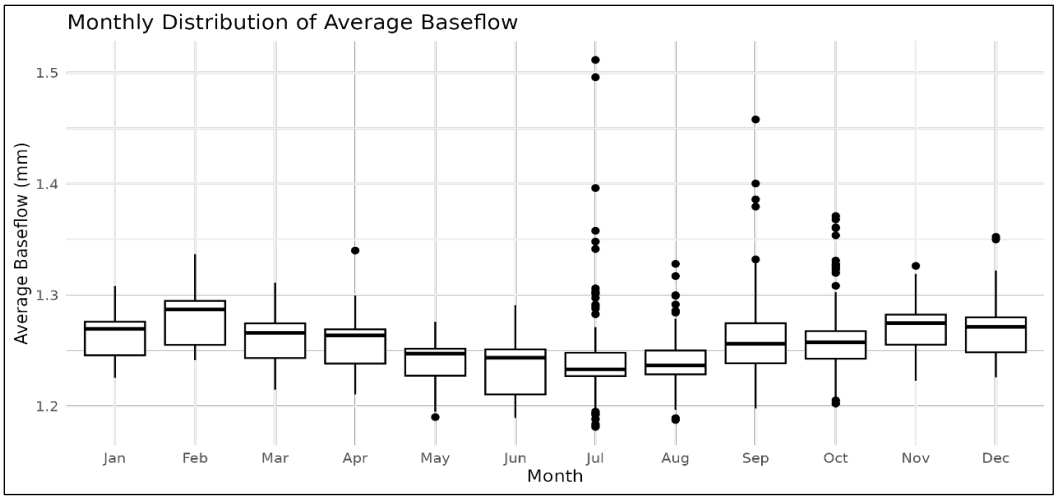

Figure 12. Boxplots of Average Monthly Baseflow.

The scatter matrix of average hydrologic metrics in Figure 13 shows that the Average Runoff (ARO) and Baseflow (ABF) are strongly right-skewed, meaning most grid cells have low fluxes and a few have very high values, while the Average Soil Moisture Storage (ASM) follows an approximate normal distribution around 200 mm. All pairwise Pearson correlations are significant ($p < 0.001$): ARO and ABF correlate weakly to moderately ($r = 0.376$), ARO and ASM moderately to strongly ($r = 0.669$), and ABF and ASM strongly ($r = 0.760$). These results reflect VIC's hydrologic behavior where, as soil moisture rises toward saturation, both surface runoff and subsurface flow increase. Scatter in the ARO-ABF relationship indicates additional controls, such as groundwater dynamics affecting baseflow. A clear threshold near 200 mm of ASM marks where runoff begins to increase rapidly, suggests that nonlinear or piecewise regression may better capture runoff generation than a simple linear model. Finally, the strong collinearity between ABF and ASM implies that including both in the same regression could lead to multicollinearity, so dimensionality reduction (for example, principal component analysis) is advisable.

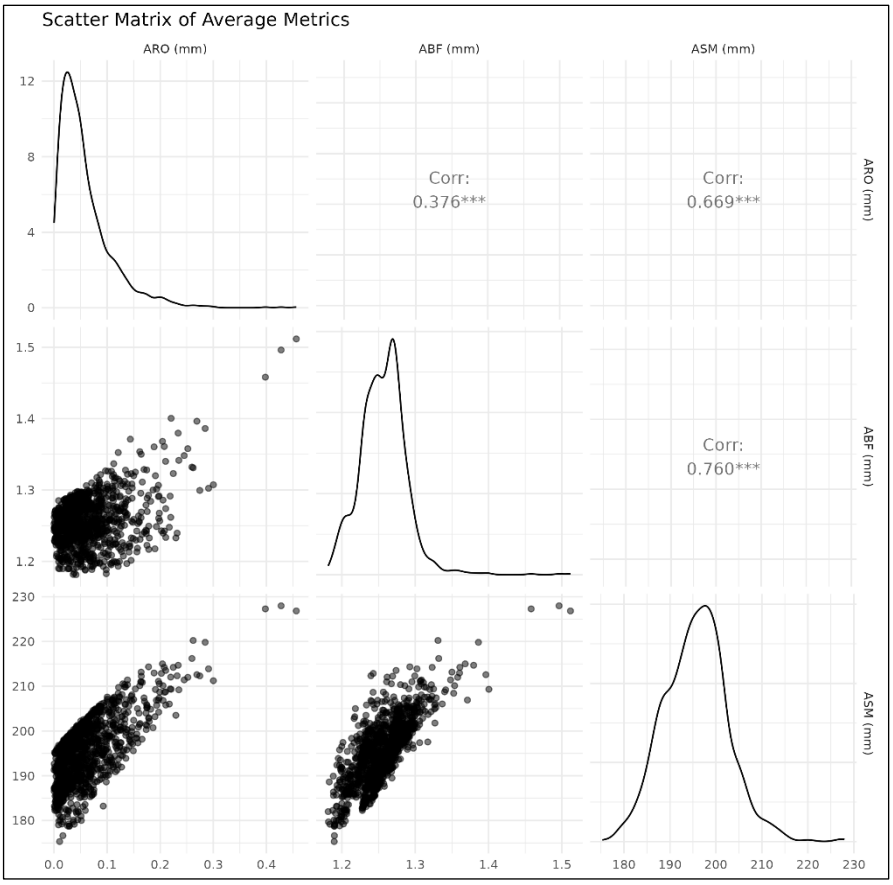

Figure 13. Scatter Matrix of Hydrologic Parameters for New Mexico.

The analysis suggests that the hydrology of New Mexico is dominated by a pronounced seasonal cycle in which modest winter precipitation gives way to a dry spring, followed by the North American Monsoon in midsummer. From December through March, median monthly rainfall lies near 0.4–0.6 mm, sustaining soil moisture at roughly 198–200 mm and baseflow at about 1.25–1.30 mm/month while generating very low runoff (<0.05 mm). As spring progresses during April–June, soil moisture falls to its annual low (~187–193 mm), baseflow declines to ~1.22–1.25 mm/month, and runoff all but vanishes (<0.03 mm). With the onset of the monsoon during July–September, median rainfall surges to 1.3–1.4 mm/month, median soil moisture gradually recovers from its early-summer minimum, reaching approximately 195–200 mm during the fall months, median baseflow remains relatively stable at approximately 1.23–1.26 mm/month, and median runoff increases to approximately 0.06–0.08 mm. These summer pulses are essential for groundwater recharge and streamflow initiation in an otherwise water-limited environment. The strong relationship between soil moisture and baseflow underscores the role of

subsurface storage in sustaining flows outside the monsoon period, while the small fraction of precipitation that becomes runoff highlights the dominance of infiltration and evapotranspiration in the regional water balance.

3.3.3. Groundwater Hydrology

The RGTIHM model provides a comprehensive view of groundwater dynamics across the LRG region for the observed period from 1940 (stress period 10) to 2014 (stress period 898), and the forecasted period until 2100 (stress period 1930) with hydraulic head and Water Table Depth (WTD) data evaluated for all the three Stress Periods (SPs) including SP 10 (in the beginning of 1941 after the transient model stabilization) and SP 898, with 2 time steps per SP representing ~15-day time step. The analysis reveals significant spatial and temporal variations across nine layers.

The modeled aquifer system beneath the LRG region exhibits a multilayered flow regime controlled by both regional gradients and localized stresses. As shown in Figure 14, the shallowest layers (Layers 1–3) maintain the highest potentiometric heads, with median values of approximately 1,150–1,230 m, reflecting recharge along the mountain front and interaction with surface water in the upstream reaches. Moving stratigraphically through Layers 4–6, median heads decline to ~1,020–1,170 m, illustrating the transition from unconfined to semi-confined conditions and reduced transmissivity in mid-aquifer sands and silts. In the deepest layers (Layers 7–9), median heads continue to decrease, while the IQRs span approximately 650–1,170 m, indicating greater confinement, lower hydraulic conductivity, and longer groundwater travel times toward, and increased spatial variability toward the distal basin. Table 2 shows that mean hydraulic heads remain relatively stable across the three selected main SPs, with differences generally less than 10 m in all layers. This result indicates that the overall groundwater system remains close to equilibrium despite localized variations within individual layers.

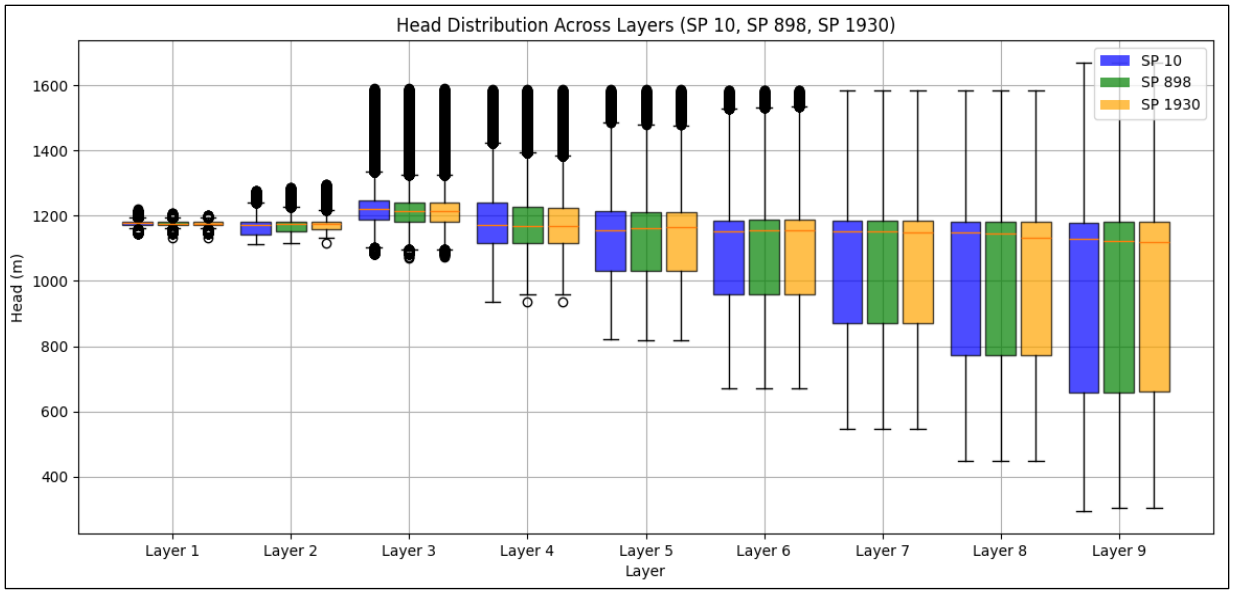

Figure 14. Boxplots of Head Distribution.

Table 2. Mean Head and Difference in Mean Head for SPs 10, 898, and 1930 for all 9 Layers. Values are rounded to the nearest meter because the converted MF6 simulation is used as a proof-of-concept framework demonstration rather than a fully recalibrated groundwater prediction model.

Layer	SP 10	SP 898	SP 1930	SP 898 − SP 10	SP 1930 − SP 10	SP 1930 − SP 898
L1	1177	1176	1175	−1	−2	−1
L2	1171	1175	1181	4	10	6
L3	1232	1223	1221	−9	−11	−2
L4	1180	1174	1173	−6	−7	−1
L5	1129	1129	1129	0	0	0
L6	1084	1084	1084	0	0	0
L7	1042	1041	1041	−1	−1	0
L8	997	995	993	−2	−4	−2
L9	944	944	945	0	1	1

Temporal changes in the head reveal both seasonal and long-term responses to irrigation pumping, river recharge, and climatic variability. Figure 15 compares early model spin-up (SP 10) to a mid-simulation period (SP 898), highlighting modest (<50 m) declines along the central valley axis, where pumping stress is greatest. By the end of the simulation (SP 1930), additional drawdown (up to 120 m) appears in the same zones, indicating cumulative depletion under sustained pumping. In contrast, near-river corridors and recharge zones along the mountain front show slight head recovery (5–20 m) during SP 1930, suggesting that monsoon-driven river infiltration partially offsets extraction.

Mid-depth aquifer responses shown in Figure 16 mirror these trends but with attenuated magnitude. Initial drawdown between SP 10 and SP 898 reaches 30–80 m under high-capacity pumping wells. Subsequent comparisons (SP 1930 vs. SP 10) show an additional 40–100 m decline, indicating slower propagation of stress into semi-confined zones. Recovery pockets remain evident near recharge boundaries, consistent with transient river-aquifer exchange during peak runoff months.

The deepest layers shown in Figure 17 exhibit the smallest net changes, with SP 10 to SP 1930 declining generally under 50 m except immediately at the down-gradient of major well fields. This pattern confirms that confined conditions and lower vertical permeability slow both depletion and recovery. Furthermore, seasonal recharge pulses impart negligible fluctuation at depth, reinforcing the notion that long-term pumping is the dominant driver for deep-aquifer head variation.

Collectively, these results indicate a vertically stratified and spatially heterogeneous aquifer system in which groundwater responses vary substantially among layers. The strongest valley-aligned response occurs in Layer 3, whereas deeper layers generally show smaller and more localized responses. Recharge during the North American Monsoon, modeled through increased river stage and infiltration, produces localized head increases in portions of the model domain. However, the simulated groundwater response remains spatially heterogeneous, reflecting the combined influences of hydrostratigraphy, structural controls, recharge, and groundwater withdrawals. These findings highlight the important of considering layer-dependent groundwater responses when evaluating long-term water-resource management strategies in the Lower Rio Grande region.

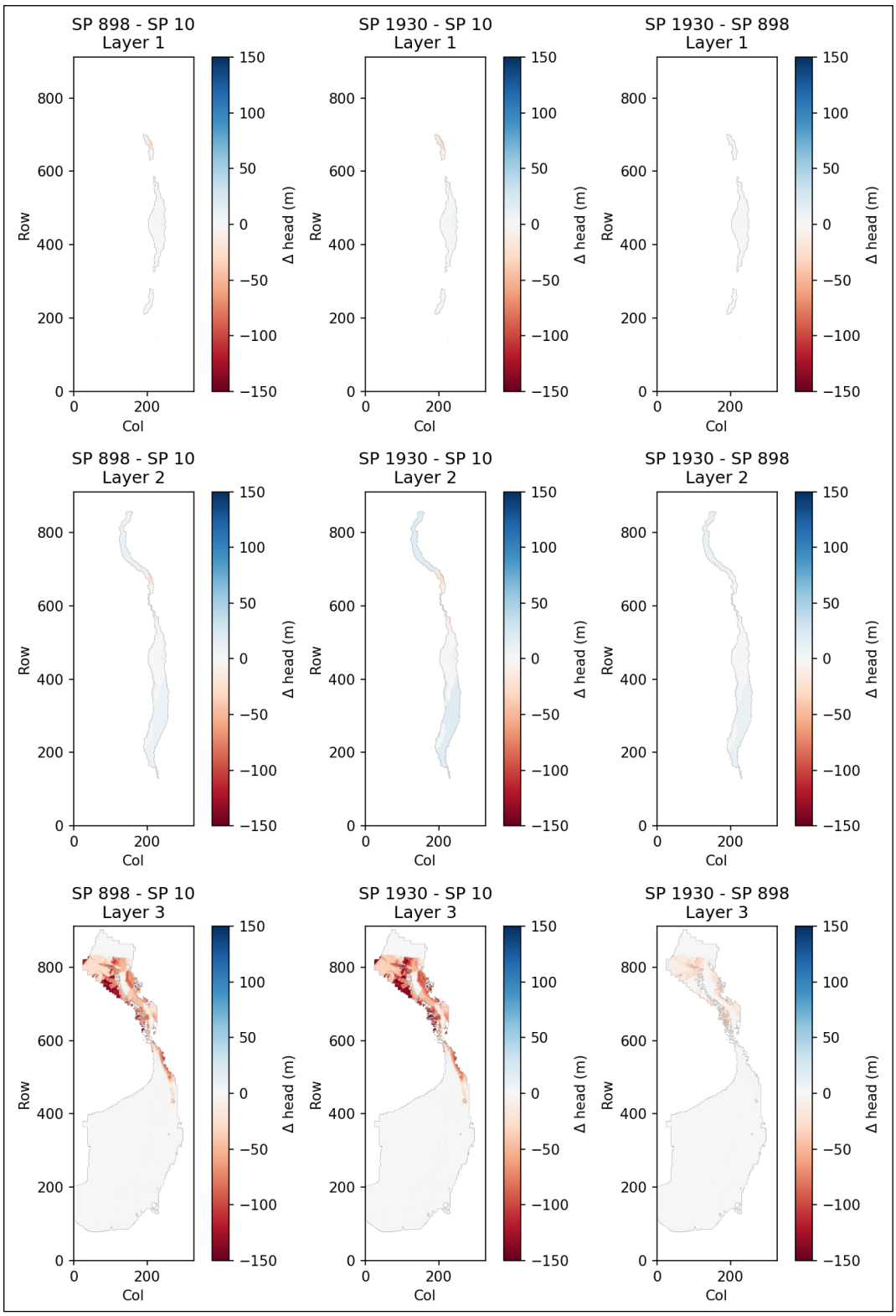

Figure 15. Head Differences Between the Start of Simulation (SP 10), End of Observation (SP 898) and End of Forecasting (SP 1930) for Layers 1–3.

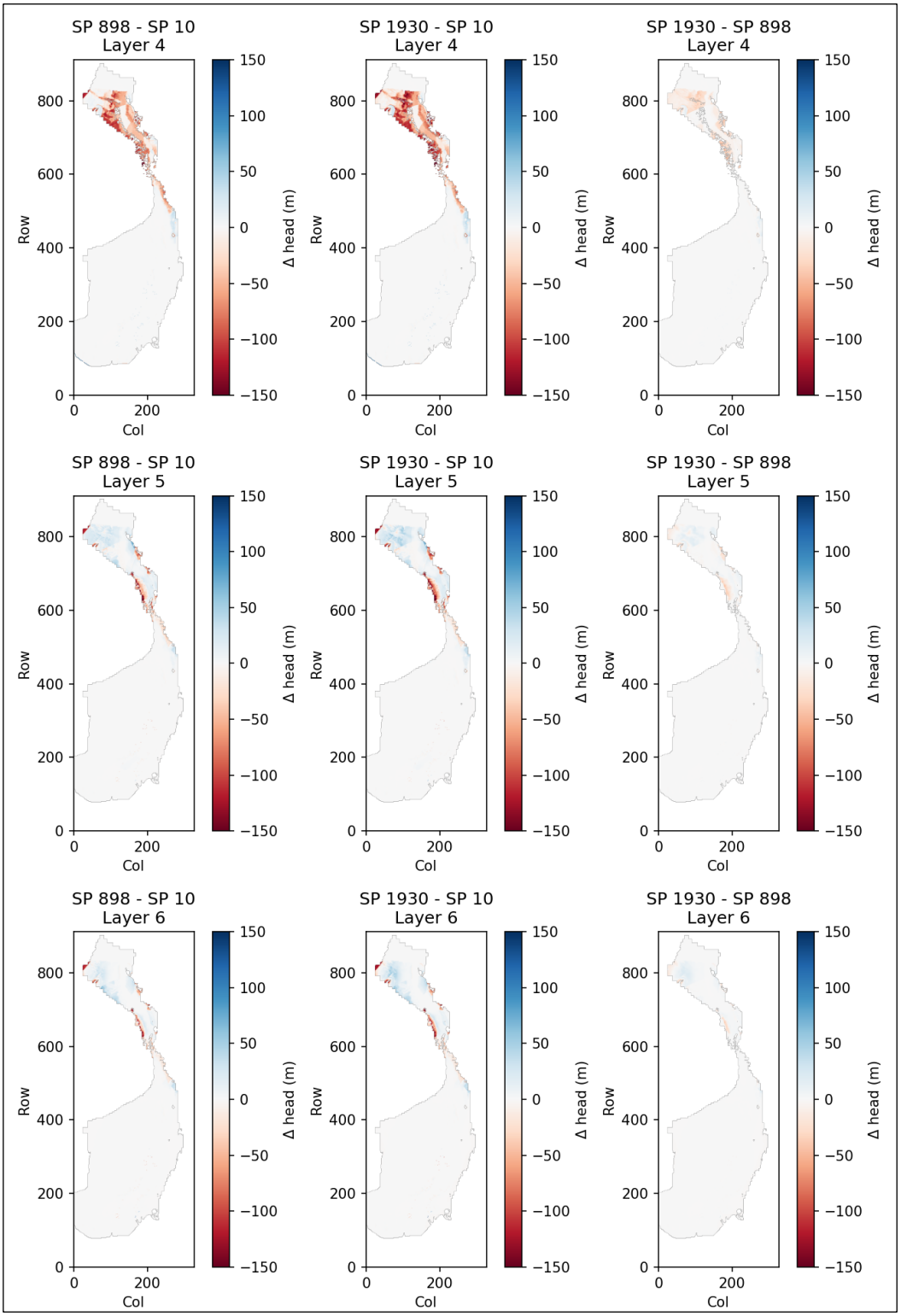

Figure 16. Head Differences Between the Start of Simulation (SP 10), End of Observation (SP 898) and End of Forecasting (SP 1930) for Layers 4–6.

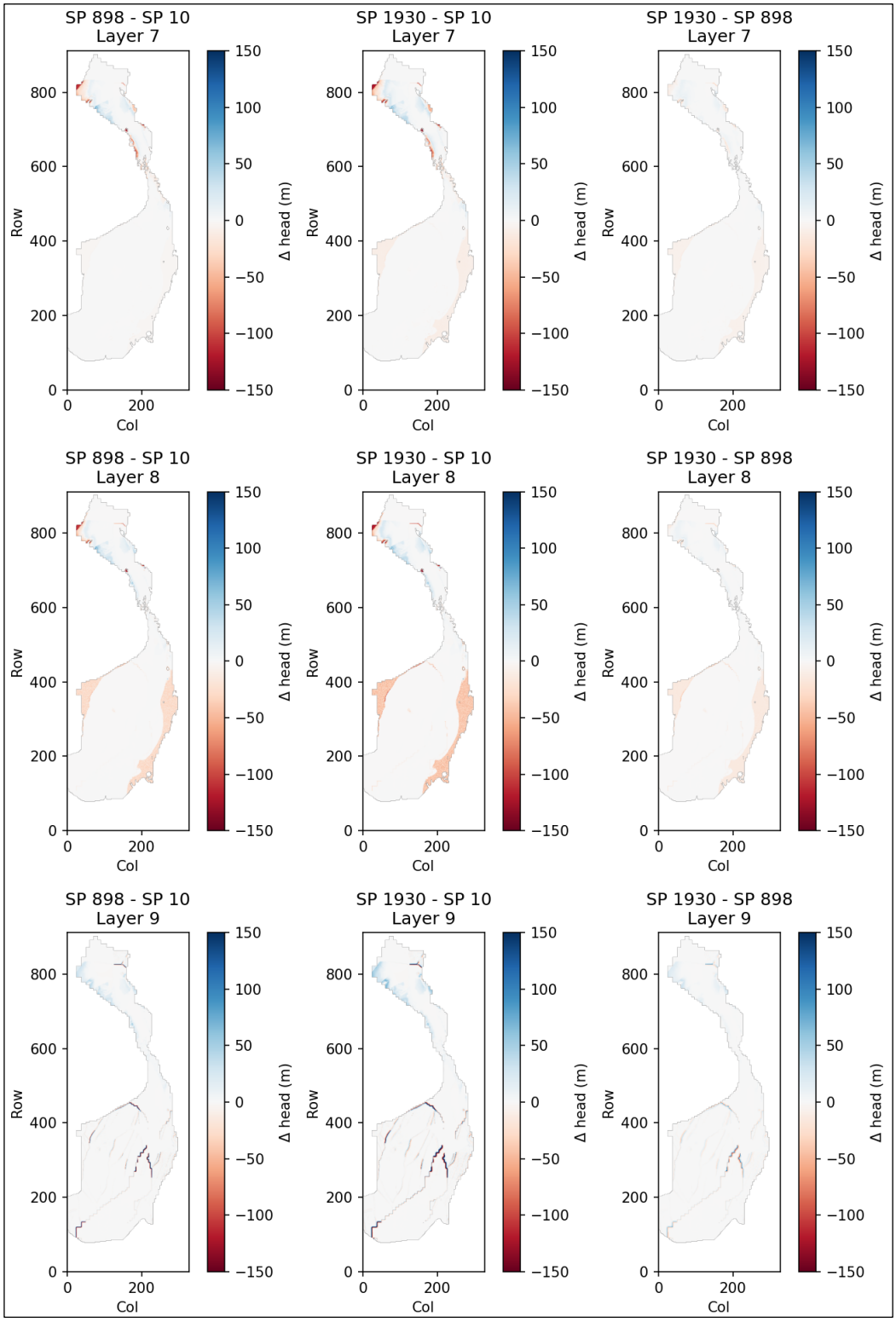

Figure 17. Head Differences Between the Start of Simulation (SP 10), End of Observation (SP 898) and End of Forecasting (SP 1930) for Layers 7–9.

3.4. Drought Vulnerability

3.4.1. Statewide Temporal Behavior

As shown in Figure 18, the statewide monthly mean DVI shows strong interannual variability. The 12-month running mean tracks multi-season anomalies and highlights pronounced drought conditions during 2011–2013, with a smaller resurgence around 2020–2021. During the 2011–2013 event, more than 50% of the state's area experienced High/Extreme drought vulnerability (DVI ≥ 0.5). After 2024, the smoothed DVI remains lower and more stable, with typical peaks below about 0.4 and the area in High/Extreme DVI usually under about 20%. These statistics summarize behavior relative to the fixed training baseline (1990–2009).

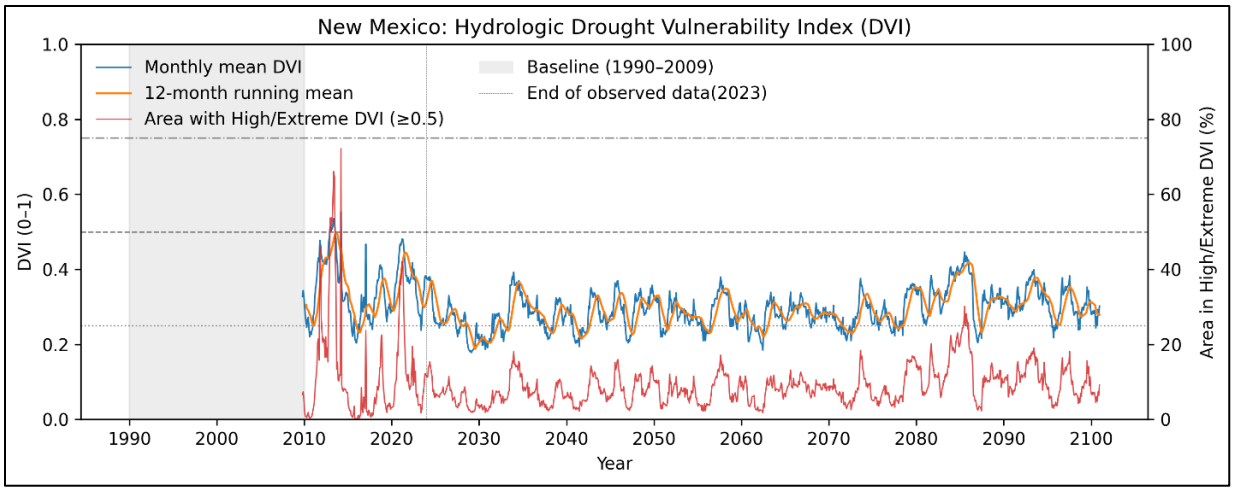

Figure 18. Statewide Monthly Mean DVI (blue), 12-Month Running Mean (orange), and Statewide Area in High/Extreme DVI (≥ 0.5, red). The shaded region marks the training baseline (1990–2009). Horizontal dashed lines indicate DVI thresholds of 0.25, 0.50, and 0.75, corresponding to increasing levels of drought vulnerability.

Figure 19 provides an observational reference from the U.S. Drought Monitor. Three statewide drought episodes are evident during 2010–2023: 2011–2013, 2018, and 2020–2021, with large coverage in the severe to exceptional categories (D3–D4). The DVI time series in Figure 18 captures all three events in timing and relative severity, with the strongest agreement during 2011–2013. This agreement indicates that the framework reproduces observed statewide drought episodes over the evaluation period.

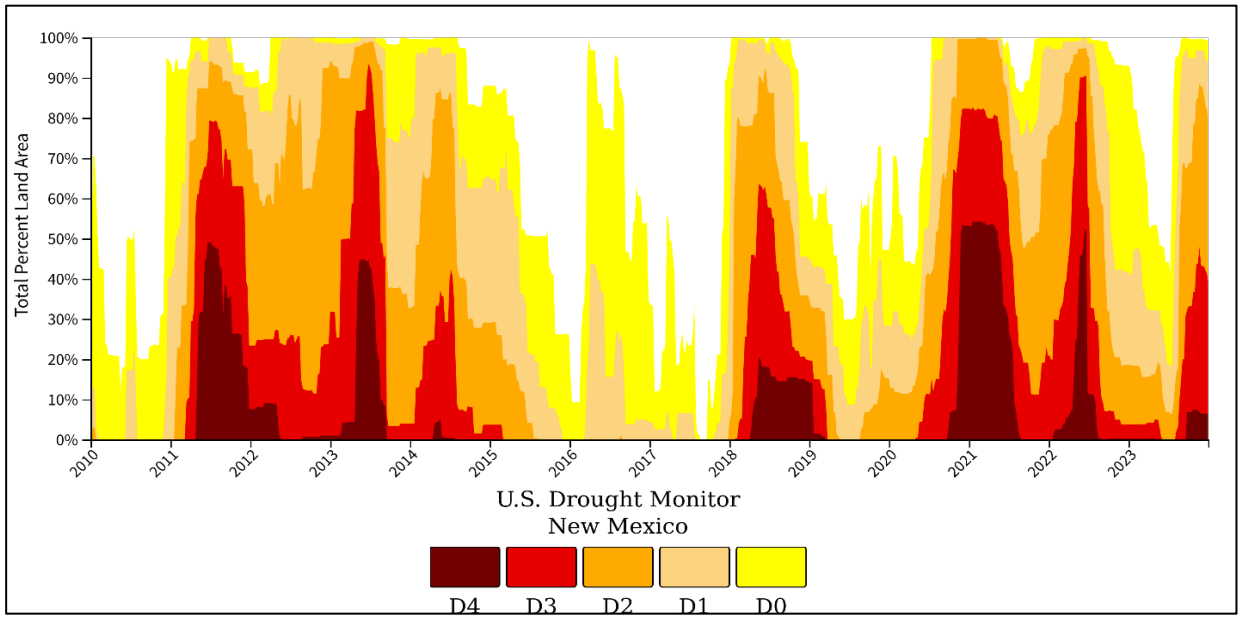

Figure 19. U.S. Drought Monitor Statewide Percent Area by Category (D0–D4) for New Mexico, 2010–2023 (source: https://www.drought.gov/).

3.4.2. Spatial Pattern of Mean Vulnerability

Mean DVI for 1991–2023 is spatially homogeneous at low to moderate levels. The future mean (2024–2100) shows higher values in the northern high terrain (for example, Sangre de Cristo and adjacent uplands) and along parts of the west-central mountains, with lower means across the central and eastern plains. The change map (future minus historical in Figure 20) is mixed: increases up to about +0.3 in portions of the northern mountains and decreases down to about −0.3 across central, south-central, and eastern New Mexico. This spatial pattern indicates a redistribution of vulnerability rather than a uniform increase.

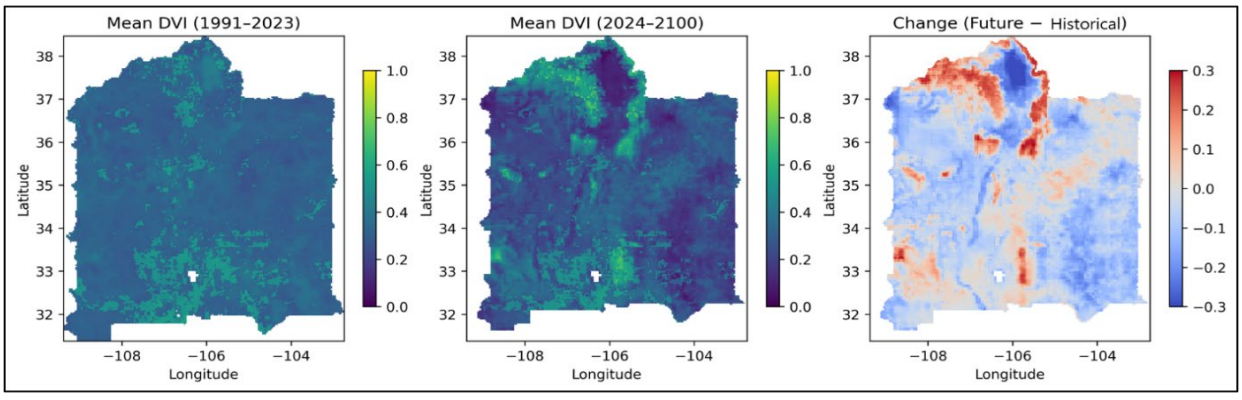

Figure 20. Mean DVI for 1991–2023 (left), Mean DVI for 2024–2100 (center), and Change (future minus historical, right).

3.4.3. Frequency of High Vulnerability (DVI ≥ 0.5)

The frequency of months with DVI ≥ 0.5 during 1991–2023 is generally low across the state, with localized hotspots. In 2024–2100, high-elevation belts in the north and west show much higher frequencies, while large areas of the central and eastern domains show little change or slight declines. The difference map (Figure 21) confirms localized increases approaching +0.5 in some mountain grids and widespread small decreases (about 0 to −0.2) elsewhere. These patterns are consistent with the mean-DVI changes and point to greater persistence of high vulnerability in snow- and runoff-dependent headwaters.

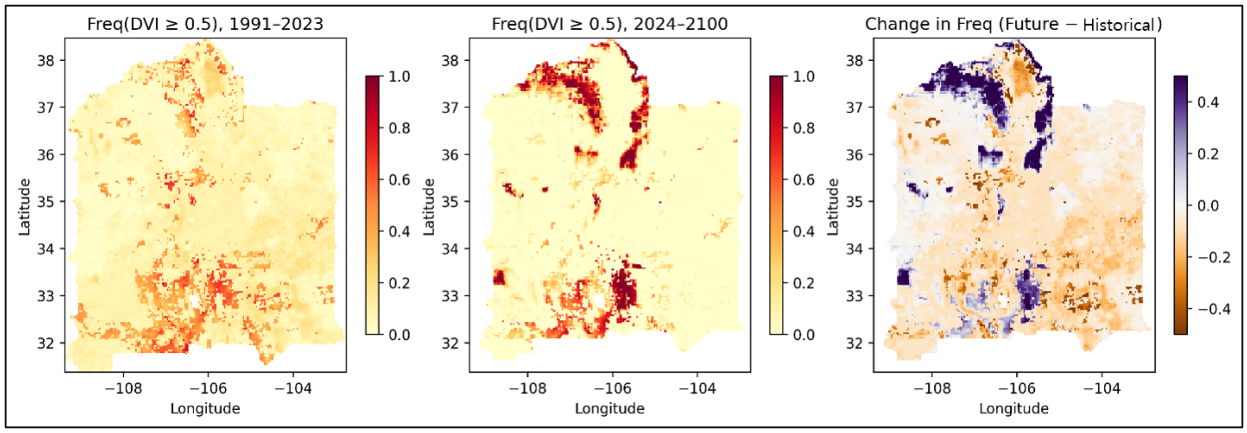

Figure 21. Frequency of Months with DVI ≥ 0.5 in 1991–2023 (left), 2024–2100 (center), and the Difference (future minus historical, right).

3.4.4. Month-to-Month Persistence of DVI Class

Area-weighted transition probabilities show strong persistence. The probability of remaining in the same class from one month to the next is 91.5% for Low, 90.7% for Moderate, 87.0% for High, and 72.6% for Extreme. Most changes are one-class steps (for example, High→Moderate 12.2%, Extreme→High 27.4%, shown in Figure 22). Direct jumps across multiple classes are rare. This persistence supports the use of backward windows and indicates that extreme vulnerability, once established, tends to relax gradually rather than abruptly.

3.4.5. Distribution Across Grid Cells

The distribution of per-cell mean DVI shifts between the two periods. The historical median is about 0.32 with a compact interquartile range. The future median is lower (about 0.26) and the spread is larger, with a longer upper tail (Figure 23). Combined with the maps, this implies a

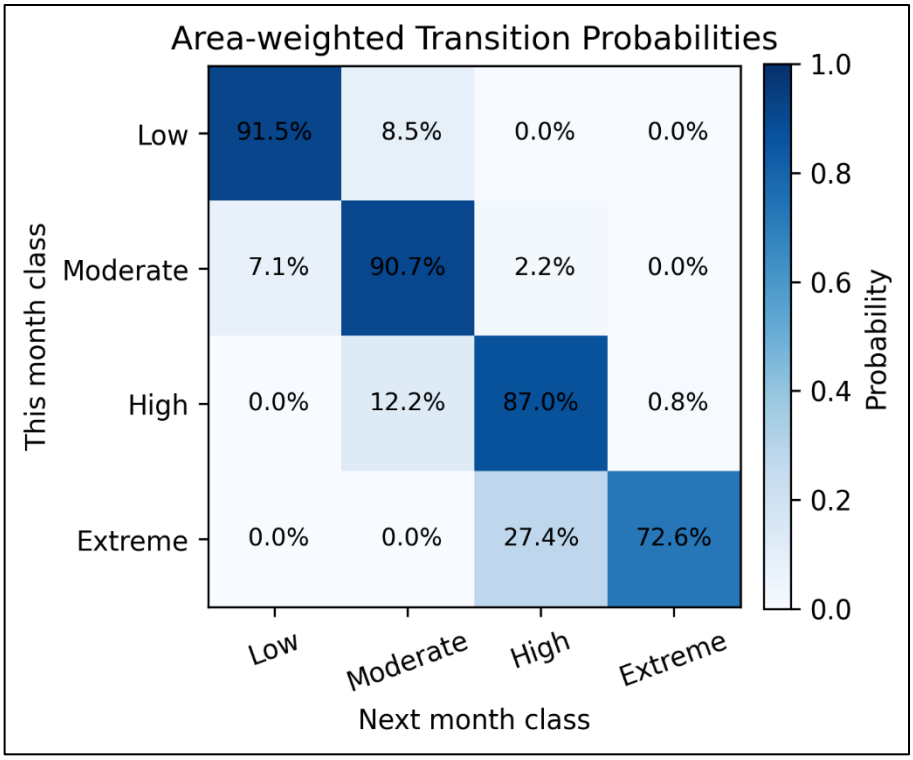

Figure 22. Area-Weighted Transition Probabilities Between Monthly DVI Classes. Rows are the current month; columns are the next month.

statewide decrease in average vulnerability but larger spatial contrasts: fewer cells at moderate levels, more cells either distinctly lower or distinctly higher, especially in northern mountain grids.

3.4.6. Synthesis

The statewide mean DVI has prominent historical peaks (2011–2013, 2020–2021) and a generally lower, steadier profile after 2024 (Figure 18). Spatially, vulnerability reorganizes rather than rises uniformly. Future increases concentrate in northern and west-central mountains, while decreases dominate central and eastern New Mexico (Figure 20). High-vulnerability months (DVI ≥ 0.5) become more frequent in headwaters but not over most plains, mirroring the mean-field changes (Figure 21). Month-to-month class persistence is high across all classes, especially Low and Moderate, indicating temporal inertia and predictability at monthly scale (Figure 22). The per-cell distribution shifts toward a lower median with greater spread, reinforcing that future vulnerability is more spatially heterogeneous even as the statewide average declines (Figure 23).

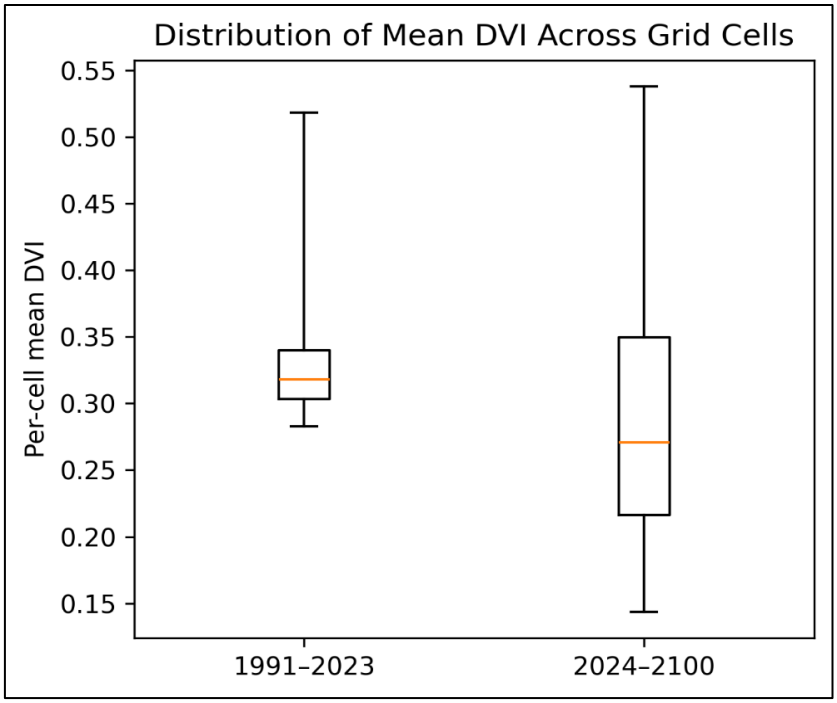

Figure 23. Distribution of Per-Cell Mean DVI for 1991–2023 and 2024–2100.

These results reflect indices standardized to the fixed 1990–2009 baseline and summarized over 1991–2023 and 2024–2100. Interpretation should focus on relative changes and spatial redistribution of vulnerability rather than absolute risk levels.

4. SOFTWARE ISSUES AND LIMITATIONS

This section summarizes the issues identified in the official MF6 and VIC software, along with potential fixes.

4.1. MF6 UZF Package Infiltration Input Overhead

The UZF package incurred significant I/O overhead when coupled with the VIC model, as infiltration was documented as finf but read as sinf from the package input file. The state variable finf was not accessible via the XMI, requiring internal conversion from sinf to finf. The MF6 documentation lists finf as the infiltration variable, but the source code treats it as a hidden state variable and reads it as sinf from the model UZF file. To resolve this, the code was updated to directly read finf, enabling VIC to pass infiltration as a state variable before each time step. This eliminated excessive file I/O, improving computational efficiency. The resolution is available at: https://github.com/MODFLOW-ORG/modflow6/compare/develop...mabdazzam:modflow6:uzf-fix.

4.2. MF6 Bottom Elevation Pass-Through Condition Errors

MF6 exhibited instability in handling pass-through conditions, where cells are marked with IDOMAIN -1. In these cases, the model attempts to identify the bottom elevation (botm) for active cells by finding the top elevation from the layer above. However, the internal routine performs only a single upward check. If the immediate layer above is inactive or missing, the model fails to find a valid top and terminates with an error.

This limitation becomes critical in models like the RGTIHM, where many geologic layers may contain gaps, Not-a-Number (NaN) values, or represent units that do not exist uniformly across the model domain. For example, in areas where Base_BSMT is the only present layer, for MF6, it may lie several layers below the nearest valid surface, with all intermediate layers being pass-through cells. In such configurations, the default logic fails to identify a valid top elevation, leading to incorrect top-bottom pairing or model crashes.

To resolve this issue, we implemented an enhanced loop that searches iteratively upward through the layer stack until a valid top is found. This valid top may come from either a non-pass-through geologic layer or the surface elevation defined by the Digital Elevation Model (DEM). By continuing the search instead of stopping at the first invalid result, the model can now assign correct top and bottom elevations even in structurally complex regions. The resolution is available at: https://github.com/MODFLOW-ORG/modflow6/compare/develop...mabdazzam:modflow6:develop. This resolution enhances MF6's reliability and efficiency in the coupled framework, supporting accurate hydrologic simulations.

4.3. MF6 Revised Indexing

Mid-study, we discontinued the MRG Basin Model because of significant challenges in converting from MF2K to MF6. The primary issue stemmed from MF6's reversed indexing system. Unlike MF2K and MF5, where the (0,0) coordinate corresponds to the upper-left corner (xul, yul), MF6 designates (0,0) as the lower-left corner (xll, yll). During the intermediate conversion through MF5, this shift caused the MRG Basin model to fail to converge. The input data, aligned with the older indexing, became misaligned with MF6's grid, and when combined with the applied IDOMAIN mask, the data went out of bounds, leading to model collapse. To include the MRG model, we either need to fix the MF5to6 converter or change the whole MRG model configuration.

4.4. NetCDF Format Conflict Between VIC and Standard Libraries

A notable compatibility issue arose during the integration of VIC with MF6, stemming from a mismatch in NetCDF file formats. The Xarray library, which relies on h5netcdf or netCDF4 Python libraries, performs optimally with NetCDF-4 files that use an HDF5 backend, making NetCDF-4 the preferred format for advanced data structures. However, VIC, by default, generates outputs in NetCDF-3 Classic or NetCDF-4 Classic format, depending on the linked NetCDF library, lacking features like compression or large file support that are available in full NetCDF-4. This format discrepancy led to errors in the coupling process, as Xarray expects NetCDF-4/HDF5, while VIC produced NetCDF-3 Classic files. Specifically, when Xarray attempted to read or write these files, it altered the file's magic bytes, resulting in "permission denied" or "file corruption" errors. This issue is exacerbated by insufficient documentation in both VIC and Xarray regarding format compatibility, increasing the risk of I/O failures.

The resolution involved updating the VIC converter to explicitly output NetCDF-4 (HDF5-backed) files, ensuring seamless compatibility with Xarray and preventing file corruption during I/O operations. This fix underscores the importance of aligning file formats in coupled modeling workflows to avoid runtime exceptions and ensure robust data handling.

4.5. Issues in Parallel Execution of the Framework

4.5.1. VIC Image Driver Parallelization Issue

The VIC model employs hybrid OpenMP and MPI parallelization, but the VIC Image Driver has an incomplete OpenMP implementation, causing data races when run with multiple processing threads (any environment variable other than OMP_NUM_THREADS=1). The fix requires a revised OpenMP implementation to ensure stable hybrid parallel execution, which is currently under development.

4.5.2. MF6 Splitter Limitations in Domain Partitioning for Parallel Simulations

The MF6 splitter cannot currently handle models containing Horizontal Flow Barriers (HFB) in parallel, a significant limitation for the RGTIHM, which extensively uses HFB. Currently, splitting the model into submodels results in imbalanced computational loads, reducing parallel efficiency. Alternatives include either accepting the imbalance or implementing HFB splitting in the MF6 splitter. Because of these unresolved issues, the framework remains sequential in nature as of now, pending further development to enable efficient parallel

execution. These resolutions and ongoing efforts to address parallel execution challenges are expected to enhance the VIC-MF6 framework's reliability, supporting accurate and efficient hydrologic simulations across New Mexico.

4.5.3. Coupled Calibration and Bias Correction

This study focused on building a coupled surface–subsurface hydrologic modeling framework and validating the coupling processes. While the surface water and groundwater models were previously calibrated independently, the coupled system may still require joint recalibration and further validation of hydrologic outputs. Additionally, because of a lack of complete observed data for certain forcing variables, two different climate models were used for meteorological forcing: MTCLIM (as suggested by the VIC documentation) for the historical period and CMIP6 for the future projections. This use of two different models for the unobserved forcing variables resulted in some inconsistencies between the two simulation periods, which are reflected in the baseflow and soil moisture trends.

5. FUTURE WORK

Our future work involves further validation and refinement of the coupled hydrologic outputs to support statewide drought vulnerability analysis, potentially through recalibration of the coupled model. Recalibration may be necessary because the original surface and groundwater models were independently calibrated without accounting for the interactions introduced through coupling. Validation against historical observations will ensure accuracy, particularly for extreme events like droughts and floods. Subsequently, we will develop a drought vulnerability index for the entire state of New Mexico, leveraging the coupled model's outputs to assess spatial and temporal risks under both historical and projected climate scenarios (up to 2100).

Additionally, building on the preliminary conversion efforts conducted during this project, future work will focus on converting and integrating the MODFLOW-2000 (MF2K) model for the Middle Rio Grande Basin (McAda and Barroll, 2002) into the current VIC-MF6 framework to expand the groundwater modeling domain beyond the Lower Rio Grande Basin. We will focus on updating its grid structure, boundary conditions, and calibration to align with modern standards. This integration of the new groundwater model into the currently coupled model will expand the modeling region for a more comprehensive statewide hydrologic analysis.

For future enhancements to the VIC-MF6 framework, we will focus on improving its scalability and applicability for statewide water resources management by implementing parallel simulations of both VIC and MF6 submodels within the coupled modeling framework. Following parallelization, the framework will be calibrated on HPC using historical data from 1940 to 2023 to optimize model parameters. Additionally, to address the discrepancy issue in the baseflow and soil moisture results between the two historical and forecasting simulation periods, we suggest the correction of systemic bias in both modeled weather forcing variables.

6. CONCLUSIONS

This study presents a fully functional coupled modeling framework linking the VIC Image Driver and MF6, establishing the foundation for integrated surface-water and groundwater simulation in New Mexico. The system runs from 1990 to 2100, capturing surface and groundwater interactions at a resolution of 1/32° and across nine vertical geologic layers within the Lower Rio Grande Basin. Model integration resolved major technical issues, including NetCDF format mismatch, problems with UZF infiltration input in MF6, and incorrect handling of vertical pass-through cells, which required source code modifications. The coupled model produces key hydrologic signals. VIC outputs reproduced the expected seasonal cycle of soil moisture, with median values declining to approximately 188–190 mm during the pre-monsoon dry period and recovering to approximately 195 – 200 mm following the onset of the summer monsoon, while monsoon-season runoff exhibited upper-quartile values approaching 0.13 mm/month. Median baseflow remains near 1.25 mm/month throughout the year, exhibiting substantially less seasonal variability than rainfall, runoff, or soil moisture. MF6 results show cumulative groundwater drawdown up to 120 m in shallow layers from 1940 to 2100, with a mean head decline of 11 m in Layer 3 and local recovery near river corridors. Deeper Layers 7–9 remain largely stable, with changes under 4 m. These results confirm that the framework captures both short-term hydrologic variability and long-term groundwater trends.

The drought vulnerability analysis complements these findings by providing an integrated assessment of climate-driven risk. The statewide DVI, constructed from VIC post-processed fields, incorporates precipitation, runoff, evapotranspiration, soil moisture, baseflow, and snowpack to represent multiple stages of hydrologic stress. Standardization against the 1990–2009 baseline enabled consistent comparisons extending through 2100. The results indicate

spatially heterogeneous changes in drought vulnerability across New Mexico, with localized increases in mean DVI and the frequency of high-vulnerability conditions in both northern and southern portions of the state. While some areas exhibit reduced vulnerability, many regions show increasing drought vulnerability under future climate conditions. Increased drought vulnerability is evident in northern mountainous regions as well as portions of central and southern New Mexico. Together, the coupled hydrologic framework and DVI provide a robust platform for evaluating water sustainability under dynamic climate conditions, supporting scenario testing, impact assessment, and targeted adaptation strategies across New Mexico's diverse hydroclimatic regions. Future work will focus on joint calibration, local climate bias correction, and expanding parallel capabilities to further strengthen statewide water resources management and planning.

PUBLICATIONS AND DISSEMINATION

Conference Presentations and Proceedings

The PI and two Research Assistants (RAs) contributed to knowledge dissemination by presenting project methodologies and results at three conferences and through one peer-reviewed conference proceeding:

- Huidae Cho, Nageena Makhdoom, November 8, 2023. *Development of a New Mexico Statewide Land Surface Model for Water Availability Analysis.* 2023 New Mexico Water Conference. Albuquerque, NM.
- Abdullah Azzam, Huidae Cho, December 12, 2024. *Coupling of Parallelized Surface Water and Groundwater Models for Statewide Hydrologic Modeling.* American Geophysical Union (AGU) 2024 Annual Meeting. Washington Convention Center, Washington, D.C.
- Huidae Cho, Abdullah Azzam, June 27, 2025. *Special Lecture: A Coupled Hydrologic Modeling Framework for Drought Evaluation in New Mexico.* GEOINFORUM-2025: The 36th General Meeting and Lecture of the Japanese Society for Geoinformatics. Osaka Metropolitan University Sugimoto Campus Science Hall, 1st floor, Building G, Osaka, Japan. (Travel supported by a different funding source).
- Huidae Cho, Abdullah Azzam, June 27, 2025. *A Coupled Hydrologic Modeling Framework for Drought Evaluation in New Mexico.* Proceedings of the 36th Conference

of the Japan Association for Information and Earth Science, pp. 001–002, 2025. https://www.jsgi.org/event/abstract/geoinforum2025/s01.pdf.

Software and Data Products

The source code and programs are available at

- https://github.com/HydroCSLab/vic-mf6/tree/vic-mf6-uzf,
- https://github.com/HydroCSLab/vic-classic-to-image,
- https://github.com/HydroCSLab/modflow6/tree/nm-hydro,
- https://github.com/HydroCSLab/rgtihm, and
- https://github.com/HuidaeCho/ispso.

The model files and data will be provided upon request because of their large size.

Workforce Development

This project directly contributed to graduate training and workforce development in hydrologic modeling and computational water resources. Two Ph.D. students were supported through Research Assistantships:

- **Nageena Makhdoom** participated in early-stage data research and VIC downscaling activities, and
- **Abdullah Azzam** carried out the core framework implementation and prepared the results for dissemination.

Through their participation, both students gained advanced skills in large-scale hydrologic modeling, climate data processing, and scientific programming. These experiences provided essential contributions to project objectives and strengthened their professional preparation for careers in computational water resources. Authorship reflects direct contributions to framework implementation, data analysis, and report preparation.

ACKNOWLEDGMENTS

This project is funded by the U.S. Geological Survey (USGS) Water Resources Research Act 104(b) grant through the New Mexico Water Resources Research Institute (NM WRRI) under award GR0007017, as part of USGS Grant/Cooperative Agreement No. G21AP10635, along with an additional internal award from the NM WRRI.

REFERENCES

Abatzoglou, J.T. (2013), Development of gridded surface meteorological data for ecological applications and modelling. *International Journal of Climatology, 33*, 121–131.

Arguez, A., & Vose, R.S. (2011). The definition of the standard WMO climate normal: The key to deriving alternative climate normals. *Bulletin of the American Meteorological Society*, *92*(6), 699–704.

Arnold, J.G., Srinivasan, R., Muttiah, R.S., & Williams, J.R. (1998). Large area hydrologic modeling and assessment part I: model development 1. *JAWRA Journal of the American Water Resources Association*, *34*(1), 73–89.

Bakker, M., Post, V., Langevin, C.D., Hughes, J.D., White, J.T., Starn, J.J., & Fienen, M.N. (2016). Scripting MODFLOW Model Development Using Python and FloPy. *Groundwater, 54,* 733–739.

Bloomfield, J.P., & Marchant, B.P. (2013). Analysis of groundwater drought building on the standardised precipitation index approach. *Hydrology and Earth System Sciences*, *17*(12), 4769–4787.

Carrão, H., Naumann, G., & Barbosa, P. (2016). Mapping global patterns of drought risk: An empirical framework based on sub-national estimates of hazard, exposure and vulnerability. *Global Environmental Change*, *39*, 108–124.

Cho, H., Kim, D., Olivera, F., & Guikema S.D. (2011). Enhanced Speciation in Particle Swarm Optimization for Multi-Modal Problems. *European Journal of Operational Research 213*(1), 15–23.

City of Las Cruces (2017). 40-Year Water Development Plan. Las Cruces Utilities. Available at https://lascruces.gov/wp-content/uploads/2024/04/40-year-Water-Plan-2017.pdf. Accessed on June 1, 2026.

Erying, V. Bony, S., Meehl, G.A., Senior, C.A., Stevens, B., Stouffer, R.J., & Taylor, K.E. (2016). Overview of the Coupled Model Intercomparison Project Phase 6 (CMIP6) experimental design and organization. *Geoscientific Model Development, 9*, 1937–1958.

Farahmand, A., & AghaKouchak, A. (2015). A generalized framework for deriving nonparametric standardized drought indicators. *Advances in Water Resources*, *76*, 140–145.

Forum, M.P. (1994). *MPI: A message-passing interface standard*. University of Tennessee.

GRASS Development Team, Landa, M., Neteler, M., Metz, M., Petrášová, A., Petráš, V., Clements, G., Zigo, T., Larsson, N., Kladivová, L., Haedrich, C., Blumentrath, S., Andreo, V., Cho, H., Gebbert, S., Nartišs, M., Kudrnovsky, H., Delucchi, L., Zambelli, P., Lennert, M., Mitášová, H., Chemin, Y., Pešek, O., Barton, M., Tawalika, C., Ovsienko, D., & Bowman, H. (2025). GRASS. https://doi.org/10.5281/zenodo.5176030. URL https://github.com/OSGeo/grass.

Gutjahr, O., Putrasahan, D., Lohmann, K., Jungclaus, J.H., von Storch, J.-S., Brüggemann, N., Haak, H., & Stössel, A. (2019). Max Planck Institute Earth System Model (MPI-ESM1.2) for the High-Resolution Model Intercomparison Project (HighResMIP), *Geoscientific Model Development, 12*, 3241–3281.

Hamman, J.J., Nijssen, B., Bohn, T.J., Gergel, D.R., & Mao, Y. (2018). The Variable Infiltration Capacity model version 5 (VIC-5): Infrastructure improvements for new applications and reproducibility. *Geoscientific Model Development*, *11*(8), 3481–3496.

Hanson, R.T., Boyce, S.E., Schmid, W., Hughes, J.D., Mehl, S.W., Leake, S.A., Maddock, T., & Niswonger, R. (2014). One-Water Hydrologic Flow Model (MODFLOW-OWHM): U.S. Geological Survey Techniques and Methods 6-A51, x, 120 p., https://doi.org/10.3133/tm6A51.

Hanson, R.T., Ritchie, A.B., Boyce, S.E., Galanter, A.E., Ferguson, I.A., Flint, L.E., Flint, A.L., & Henson, W.R. (2020). *Rio Grande transboundary integrated hydrologic model and water-availability analysis, New Mexico and Texas, United States, and northern Chihuahua, Mexico*. US Geological Survey. https://doi.org/10.3133/sir20195120.

Harbaugh, A.W. (2007). MF2KtoMF05UC, a program to convert MODFLOW-2000 files to MODFLOW-2005 and UCODE_2005 files: U.S. Geological Survey Open-File Report 2007–1204, 4 p., https://doi.org/10.3133/ofr20071204.

Hughes, J.D., Russcher, M.J., Langevin, C.D., Morway, E.D., & McDonald, R.R. (2022). The MODFLOW Application Programming Interface for simulation control and software interoperability. *Environmental Modelling & Software*, *148*, 105257.

Hungerford, R.D., Nemani, R.R., Running, S.W., & Coughlan, J.C. (1989). MTCLIM: a mountain microclimate simulation model. Res. Pap. INT-RP-414. Ogden, UT: U.S. Department of Agriculture, Forest Service, Intermountain Research Station. 52 p.

Hutton, E.W.H., Piper, M.D., & Tucker, G.E. (2020). The Basic Model Interface 2.0: A standard interface for coupling numerical models in the geosciences. *Journal of Open Source Software, 5*(51), 2317.

Institute of Electrical and Electronics Engineers (IEEE) (2024) IEEE Std 1003.1-2024: IEEE/Open Group Standard for Information Technology—Portable Operating System Interface (POSIX™) Base Specifications, Issue 8.

Jafari, T., Kiem, A.S., Javadi, S., Nakamura, T., & Nishida, K. (2021). Fully integrated numerical simulation of surface water-groundwater interactions using SWAT-MODFLOW with an improved calibration tool. *Journal of Hydrology: Regional Studies*, *35*, 100822.

Ketchum, D.G. (2016). *High-resolution estimation of groundwater recharge for the entire state of New Mexico using a soil-water-balance model*. New Mexico Institute of Mining and Technology.

Langevin, C.D., Hughes, J.D., Banta, E.R., Provost, A.M., Niswonger, R.G., & Panday, S. (2017). MODFLOW 6 modular hydrologic model: US Geological Survey Software. *US Geological Survey*.

Liang, X., Lettenmaier, D.P., Wood, E.F., & Burges, S.J. (1994). A simple hydrologically based model of land surface water and energy fluxes for general circulation models. *Journal of Geophysical Research: Atmospheres*, *99*(D7), 14415–14428.

Maurer, E.P., Wood, A.W., Adam, J.C., Lettenmaier, D.P., & Nijssen, B. (2002). A long-term hydrologically based dataset of land surface fluxes and states for the conterminous United States. *Journal of Climate*, *15*(22), 3237–3251.

McAda, D.P., & Barroll, P. (2002). *Simulation of ground-water flow in the Middle Rio Grande basin between Cochiti and San Acacia, New Mexico* (Vol. 2, Issue 4200). US Department of the Interior, US Geological Survey.

McKee, T.B., Doesken, N.J., & Kleist, J. (1993). The relationship of drought frequency and duration to time scales. *Proceedings of the 8th Conference on Applied Climatology*, *17*(22), 179–183.

National Oceanic and Atmospheric Administration (NOAA), (1976). *US Standard Atmosphere, 1976* (NOAA-S/T-76-1562).

Naumann, G., Barbosa, P., Garrote, L., Iglesias, A., & Vogt, J. (2014). Exploring drought vulnerability in Africa: an indicator based analysis to be used in early warning systems. *Hydrology and Earth System Sciences*, *18*(5), 1591–1604.

PRISM Climate Group, Oregon State University (2026). https://prism.oregonstate.edu, accessed May 26, 2026.

Shukla, S., & Wood, A.W. (2008). Use of a standardized runoff index for characterizing hydrologic drought. *Geophysical Research Letters*, *35*(2).

Sridhar, V., Billah, M.M., & Hildreth, J.W. (2018). Coupled surface and groundwater hydrological modeling in a changing climate. *Groundwater*, *56*(4), 618–635.

Svoboda, M., LeComte, D., Hayes, M., Heim, R., Gleason, K., Angel, J., Rippey, B., Tinker, R., Palecki, M., & Stooksbury, D. (2002). The drought monitor. *Bulletin of the American Meteorological Society*, *83*(8), 1181–1190.

Sweetkind, D.S. (2017). *Three-dimensional hydrogeologic framework model of the Rio Grande transboundary region of New Mexico and Texas, USA, and northern Chihuahua, Mexico*. US Geological Survey.

Union of Concerned Scientists (2016). *Confronting Climate Change in New Mexico*. 1–14.

Van Loon, A.F. (2015). Hydrological drought explained. *Wiley Interdisciplinary Reviews: Water*, *2*(4), 359–392.

Vicente-Serrano, S.M., Beguería, S., & López-Moreno, J.I. (2010). A multiscalar drought index sensitive to global warming: the standardized precipitation evapotranspiration index. *Journal of Climate*, *23*(7), 1696–1718.

Xu, F. (2018). *Estimation of focused recharge for New Mexico using a soil-water-balance model: PyRANA*. New Mexico Institute of Mining and Technology.

Yang, Y., Pan, M., Beck, H.E., Fisher, C.K., Beighley, R.E., Kao, S., Hong, Y., & Wood, E.F. (2019). In quest of calibration density and consistency in hydrologic modeling: Distributed parameter calibration against streamflow characteristics. *Water Resources Research*, *55*(9), 7784–7803.

New Mexico Water Resources Research Institute
3170 S. Espina Street
New Mexico State University
Las Cruces, NM 88003-8001

(575) 646-4337 • nmwrri@nmsu.edu